Cell Reports

Article

Alzheimer's genetic risk factor Bin1 controls synapse vesicle exo-endocytosis in inhibitory synapses

Graphical abstract

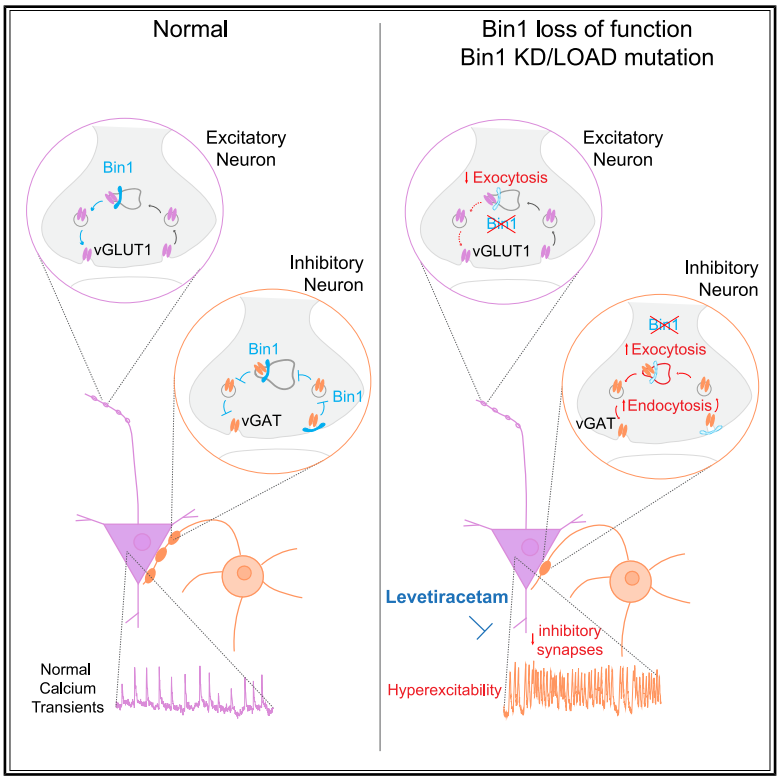

Highlights

- Bin1 is more crucial in the SV cycle of inhibitory than excitatory synapses
- Bin1 loss reduces inhibitory synapses and contributes to hyperexcitability
- Alzheimer's disease-associated Bin1 mutations recapitulate Bin1 loss of function
- Levetiracetam rescues inhibitory synapses and hyperexcitability due to BIN1 loss

Authors

Mariana A. Barata, Catarina Perdigão, José Ramalho, Edgar R. Gomes, Cláudia Guimas Almeida

Correspondence

claudia.almeida@nms.unl.pt

In brief

Barata et al. show that the Alzheimer's risk gene BIN1 is critical for the stability of inhibitory synapses. BIN1 deficiency accelerates the synaptic vesicle endocytic cycle, leading to synapse loss and neuronal hyperexcitability, a phenotype reversed by the antiepileptic drug levetiracetam.

Barata et al., 2025, Cell Reports *44*, 116005
August 26, 2025
https://doi.org/10.1016/j.celrep.2025.116005

CellPress

Cell Reports

CellPress
OPEN ACCESS

Article

Alzheimer's genetic risk factor Bin1 controls synapse vesicle exo-endocytosis in inhibitory synapses

Mariana A. Barata,[1,5] Catarina Perdigão,[1,2,5] José Ramalho,[1] Edgar R. Gomes,[3,4] and Cláudia Guimas Almeida[1,6,*]
[1]iNOVA4Health, NOVA Medical School, Universidade Nova de Lisboa, 1169-056 Lisboa, Portugal
[2]Max Planck Institute for Multidisciplinary Sciences, Department Molecular Neurobiology, 37077 Göttingen, Germany
[3]Gulbenkian Institute for Molecular Medicine, Avenida Professor Egas Moniz, 1649-035 1649-028 Lisbon, Portugal
[4]Faculdade de Medicina, Universidade de Lisboa, Avenida Professor Egas Moniz, 1649-028 Lisbon, Portugal
[5]These authors contributed equally
[6]Lead contact
*Correspondence: claudia.almeida@nms.unl.pt
https://doi.org/10.1016/j.celrep.2025.116005

SUMMARY

BIN1, a late-onset Alzheimer's disease (LOAD) risk gene, is an endocytic regulator with an unclear synaptic function. We find Bin1 more prominently in inhibitory synapses (vGAT positive) than in excitatory ones (vGLUT1 positive). Bin1 knockdown reduces inhibitory synapses independently of Aβ42 production, increasing GABA release from the remaining synapses due to accelerated vGAT exocytosis and endocytosis, which decreases the size of inhibitory synaptic endosomes. In excitatory synapses, Bin1 only reduces vGLUT1 exocytosis. LOAD Bin1 mutants cannot compensate for the loss of inhibitory synapses, suggesting that these mutations are pathogenic. A loss of Bin1 function increases neuronal calcium levels and hyperexcitability, leading to elevated glutamate release due to lack of inhibition. Levetiracetam, an antiepileptic targeting presynaptic mechanisms, mitigates inhibitory synapse loss and hyperexcitability. Our findings show that Bin1 is an endocytic regulator of inhibitory synapses, link Bin1 dysfunction to neuronal hyperexcitability that contributes to Alzheimer's disease-related seizures, and emphasize levetiracetam's therapeutic potential.

INTRODUCTION

Synapse loss best correlates with cognitive decline in Alzheimer's disease (AD).[1,2] Therefore, identifying the underlying mechanisms of synapse dysfunction in AD should become a major therapeutic target. Dysfunction of excitatory synapses contributes to reduced long-term potentiation, which explains memory deficits in AD.[3–5] Conversely, defects in inhibitory synapses contribute to neuronal hyperexcitability, which explains hyperactivity and seizures in AD, potentially preceding the loss of excitatory synapses and the onset of memory loss.[4,6–10]

In early-onset familial AD, monogenic mutations deregulate beta-amyloid (Aβ) production and potentiate aggregation, which affect excitatory[6,11–18] and inhibitory synapses.[6,19,20] In late-onset AD (LOAD), whether the risk genes cause synapse dysfunction directly or indirectly via increased Aβ production is unclear. Notably, many LOAD risk genes function in endocytic trafficking, which is critical for synapses[21] and linked to endosomal abnormalities characterizing early LOAD pathology.[22] The endocytic regulator bridging integrator 1, Bin1, is a major risk factor for LOAD.[23,24] Bin1 is a BAR domain protein that enables membrane scission with a neuronal-specific isoform.[25]

We and others have implicated Bin1 in the endocytic production of Aβ42[26–28] by enabling the scission of BACE1-tubular recycling carriers from early endosomes in axons. Bin1 knockdown (KD) led to BACE1 endosomal accumulation, higher amyloidogenic activity, and intraneuronal Aβ accumulation.[26] Moreover, we found that mutations in *BIN1* associated with LOAD, rs754834233 (p.Pro318Leu[29] [PL]) and rs138047593 (p.Lys542Arg[30] [KR]), cause Bin1 loss of function in amyloidogenesis.[27] *In vivo*, the KD of Bin1 did not lead to the formation of extracellular amyloid plaques.[31] However, it did impact synaptic transmission,[32–35] indicating that Bin1 loss of function may affect synapses independently of Aβ. Indeed, two previous studies suggest that Bin1 regulates the synaptic vesicle (SV) cycle,[36] especially SV release in excitatory neurons.[32,36] After SV release, SV endocytic recycling involves compensatory endocytosis and SV reformation from an intermediate endosomal compartment, which requires scission and may depend on Bin1 activity. Moreover, we hypothesized that Bin1 regulation of the endocytic trafficking implicated in the SV cycle might be disrupted by LOAD mutations, leading to synapse dysfunction. Here, we assessed the function of Bin1 in synapses using primary cultures of mouse cortical neurons. Unexpectedly, we discovered that Bin1's primary function is in inhibitory synapses, where it regulates SV exocytosis and endocytosis. The LOAD mutations in Bin1 impaired its synaptic function, insensitive to Aβ inhibition. Bin1 KD reduced inhibitory transmission, leading to neuronal hyperexcitability. By decreasing the

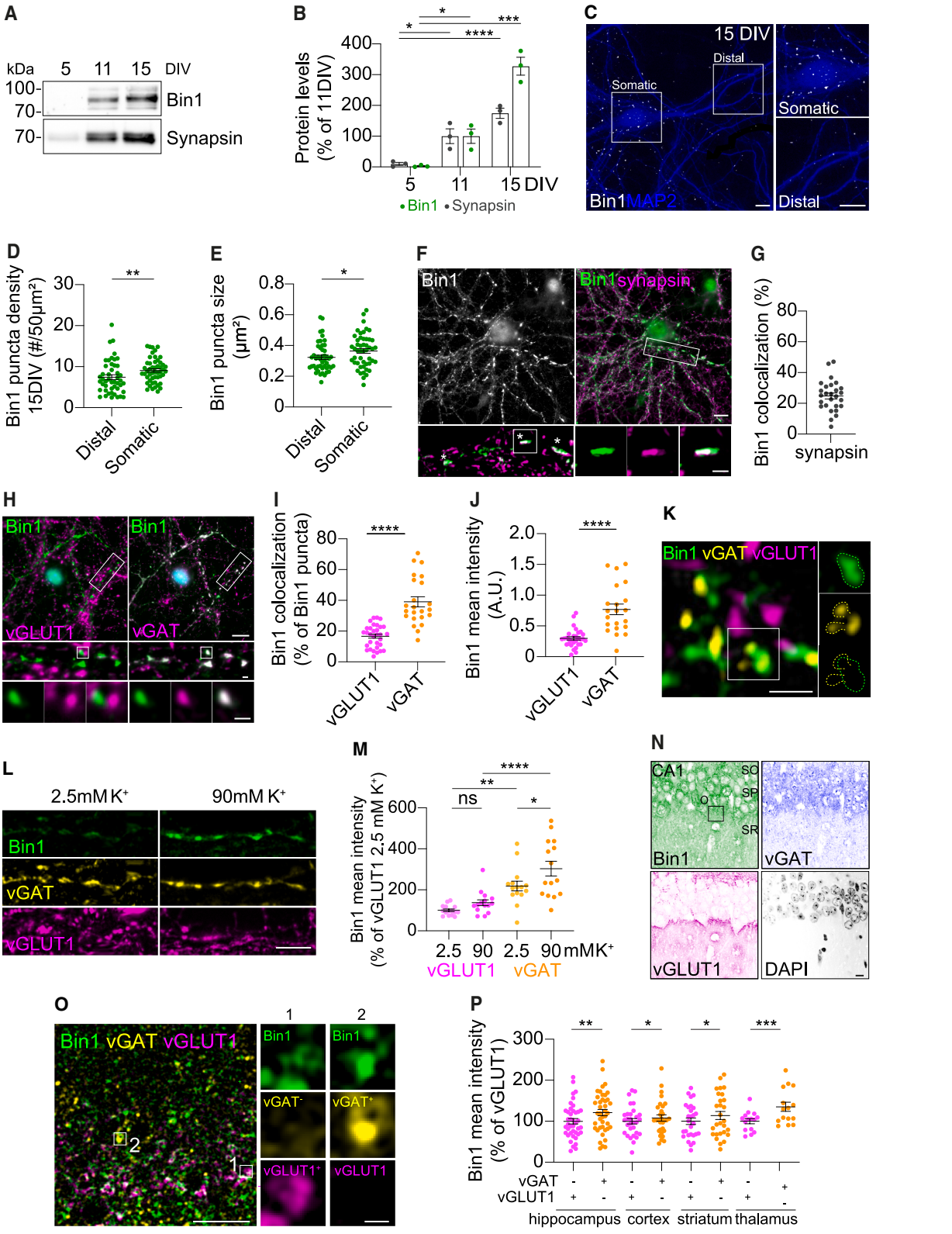

(legend on next page)

threshold for the development of seizures, *BIN1* risk variants may contribute to AD development.

RESULTS

Bin1 localizes predominantly at inhibitory presynaptic boutons

Bin1 has been localized both to presynaptic boutons[32,36,37] and postsynaptically.[34,38] Using western blot analysis of synaptosomal fractions prepared from adult mouse brains through sequential centrifugation, we detected Bin1 (anti-Bin1 99D antibody) more prominently in the presynaptic fraction, enriched in synapsin I, and absent in the postsynaptic fraction, enriched in PSD-95 (Figures S1A and S1B).

As synaptic maturation progressed, levels of Bin1 increased in primary mouse embryonic cortical and hippocampal neurons over time in culture (5–15 days in vitro [DIV]), as shown by western blot (Figures 1A and 1B). Immunofluorescence revealed that Bin1 became increasingly concentrated in puncta resembling synaptic boutons, whose density increased as neurons matured synaptically (Figures S1C and S1D). We also observed that Bin1 puncta were more numerous and larger in the perisomatic regions compared to the distal regions of the neurons (Figures 1C–1E), suggesting Bin1 prevails in a subset of synapses.

We found that 25% of Bin1 puncta colocalize with synapsin I, present in all synapses (Figures 1F and 1G). To determine whether Bin1 was more prevalent in a specific synaptic subtype, we analyzed the colocalization of Bin1 with the presynaptic excitatory marker vesicular glutamate transporter 1 (vGLUT1) and the inhibitory marker vesicular GABA transporter (vGAT) in mature neurons (Figure 1H). Bin1 was twice more abundant in inhibitory presynaptic compartments, with 40% colocalizing with vGAT and only 17% with vGLUT1 (Figure 1I). Additionally, the Bin1 levels were over 2-fold higher in vGAT puncta (Figure 1J). Also, 31% of vGAT and only 13% of vGLUT1 colocalized with Bin1 (Figure S1E). Super-resolution imaging of a Bin1-positive vGAT synaptic punctum revealed two small vGAT-positive puncta juxtaposed to a larger Bin1-positive vesicle, suggesting that two SVs were budding from an endosome (Figure 1K). We also assessed the colocalization of Bin1 with PSD-95 and gephyrin, postsynaptic excitatory, and inhibitory proteins, respectively (Figure S1F). Bin1 colocalized similarly with postsynaptic PDS-95 and gephyrin (17%) (Figure S1G), consistent with a postsynaptic role.[34]

Given the synaptic localization of Bin1, we hypothesized that it might be controlled by neuronal activity. To test this hypothesis, we analyzed Bin1 localization in axons and in inhibitory and excitatory synapses after neuronal depolarization with a high-potassium solution (Figure 1L). We found a 30% increase in Bin1 mean intensity in stimulated axons and, interestingly, a higher increase in Bin1 levels in vGAT-positive synapses compared to vGLUT-positive synapses (Figures S1H and S1M). These results suggest that the localization of Bin1 to inhibitory synapses may be regulated by synaptic activity, a finding that warrants further investigation.

Next, we evaluated the synaptic localization of Bin1 in the brain. We found that the Bin1 mean intensity was higher in the cortex and thalamus (Figures S1I and S1J). Interestingly, in the AD-relevant *cornu ammonis* 1 (CA1) region of the mouse hippocampus (Figure 1N), Bin1 and vGAT immunostaining were predominant in the stratum pyramidal (SP) layer, whereas vGLUT1 was predominant in the *stratum radiatum* layer. Comparable segregation of the Bin1 signal with vGAT was observed in the dentate gyrus (DG) (Figure S1K). At higher magnification, Bin1 was found to be more enriched in vGAT puncta than in vGLUT1 puncta, as measured by the relative mean intensity of Bin1 per synaptic puncta in the hippocampus, cortex, striatum, and thalamus (Figures 1O and 1P). No difference was detected by colocalization analysis, probably due to the high density of synapses in the brain (Figure S1L).

In culture and the brain, we detected Bin1 predominantly in the perisomatic region of excitatory pyramidal neurons, enriched in vGAT-positive puncta, consistent with an important localization of Bin1 in axo-somatic inhibitory synapses.

Our data support that Bin1 is predominantly an inhibitory presynaptic protein.

Bin1 KD reduces inhibitory synapses

The synaptic localization of Bin1 led us to use a KD approach to investigate the role of Bin1 in excitatory and inhibitory synapses (Figure 2). Bin1 levels were downregulated in mature neurons (15

Figure 1. Bin1 localizes mostly at somatic inhibitory presynaptic boutons

(A and B) Bin1 with synaptic maturation. (A) Bin1 and synapsin I levels in primary neurons after 5, 11, and 15 DIV. (B) Levels normalized to 11 DIV. $n = 3$; $^{*}p = 0.0138$ $Bin1_{11DIV}$ vs. $Bin1_{5DIV}$, $^{****}p < 0.0001$ $Bin1_{15DIV}$ vs. $Bin1_{5DIV}$; $^{*}p = 0.0210$ $synapsin_{11DIV}$ vs. $synapsin_{5DIV}$, $^{***}p = 0.0005$ $synapsin_{15DIV}$ vs. $synapsin_{5DIV}$; two-way ANOVA.

(C–E) Bin1 puncta along MAP2 dendrites. (C) Quantification of Bin1 puncta density (D) and puncta size (E) in distal vs. somatic regions in 15 DIV neurons. Scale bar, 10 μm. 3 independent experiments; $n = 47–50$ neurites; $^{**}p = 0.0069$ (D); $^{*}p = 0.0315$ (E); Mann-Whitney test.

(F–J) Bin1 colocalization with presynaptic markers in primary neurons. (F) Immunofluorescence of Bin1 and synapsin I. (H) Immunofluorescence of Bin1, vGLUT1, and vGAT. Scale bars, 10 μm, 1 μm (insets). (G and I) Quantification of Bin1 colocalization. (J) Mean intensity of Bin1 in vGAT+ or vGLUT1+ puncta. 3–4 independent experiments, $n = 21–32$ neurites. Unpaired t test (I), Mann-Whitney test (J). $^{****}p < 0001$.

(K) Super-resolution image of Bin1 with vGAT and vGLUT1. Scale bar, 1 μm.

(L and M) Synaptic Bin1 immunofluorescence after stimulation (90 mM KCl) compared to control (2.5 mM KCl). Scale bar, 5 μm. (L) Mean intensity of Bin1 in vGAT+ or vGLUT1+ puncta (M). 3 independent experiments; $n = 15$ neurites, ordinary one-way ANOVA, $^{*}p = 0.0329$ (90 mM vs. 2.5mM, vGAT), $^{**}p = 0.0022$ (vGLUT1 vs. vGAT, 2.5mM), $^{****}p < 0.0001$ (vGLUT1 vs. vGAT, 90 mM). ns, non-significant.

(N–P) Bin1 localization with presynaptic markers in mouse hippocampus (CA1). Immunohistochemistry (N and O) and quantification (P) of Bin1 mean intensity in vGLUT1 and vGAT puncta. SO, *stratum oriens*; SP, *stratum pyramidale*; SR, *stratum radiatum*. Scale bar, 10 μm, 5 μm (inset), 0.5 μm (synaptic puncta). Synaptic puncta (1) Bin1 in $vGAT^{-}vGLUT1^{+}$ puncta and (2) $vGAT^{+}vGLUT1^{-}$ puncta. 3 independent experiments; $n = 15–41$ images; $^{**}p = 0.0034$ $hippocampus_{vGAT}$ vs. $hippocampus_{vGLUT1}$, $^{*}p = 0.0162$ $cortex_{vGAT}$ vs. $cortex_{vGLUT1}$, $^{*}p = 0.0281$ $striatum_{vGAT}$ vs. $striatum_{vGLUT1}$, $^{***}p = 0.0003$ $thalamus_{vGAT}$ vs. $thalamus_{vGLUT1}$; Wilcoxon test.

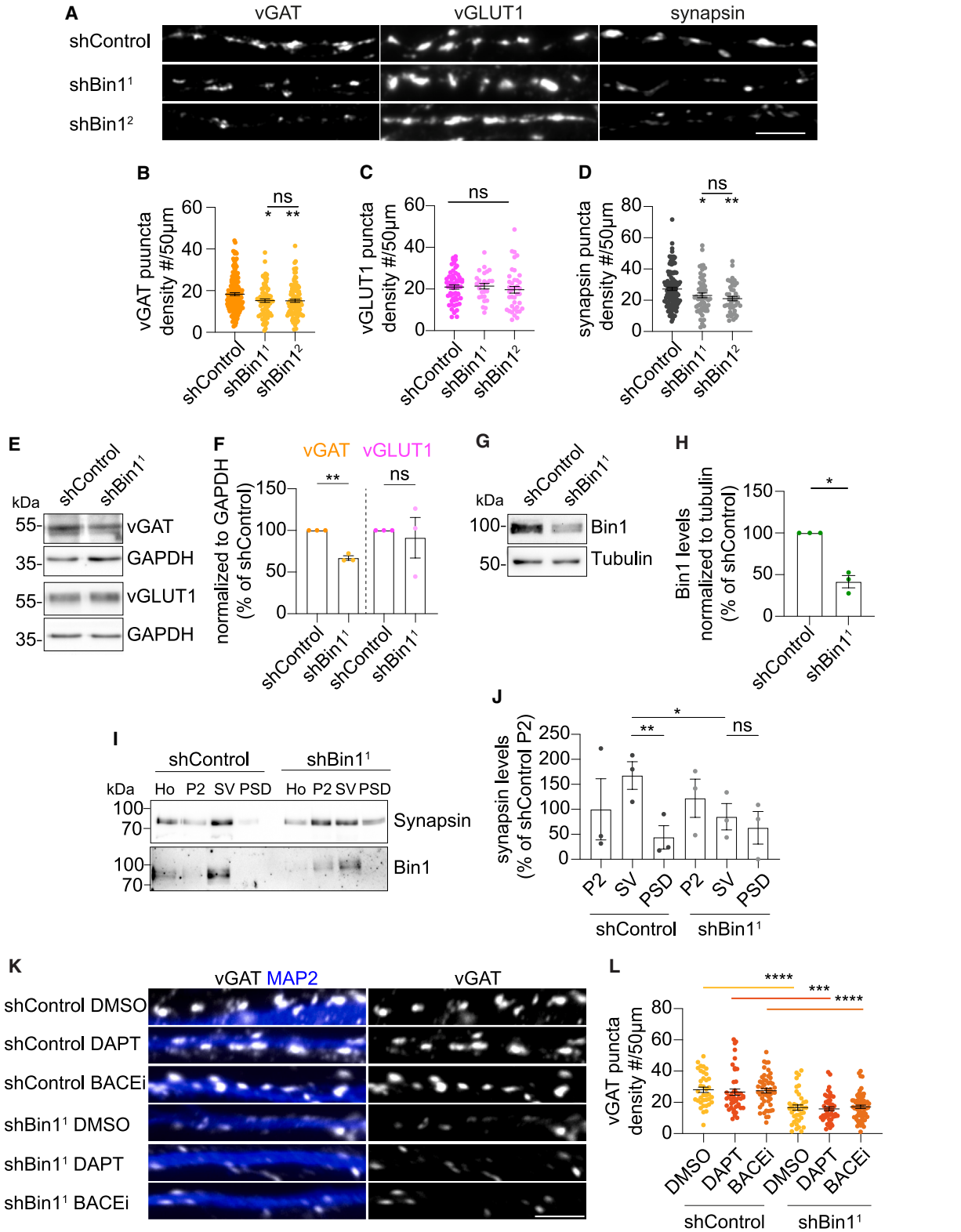

(legend on next page)

DIV) with two out of three short hairpin RNA (shRNA) sequences targeting Bin1 tested (shBin1) (Figures S2A–S2D), which lowered the mean intensity of Bin1 (Figures S2E and S2F) without impacting dendritic length or branching (Figures S2G and S2H) compared to non-targeting shRNA (shControl).

We analyzed the density of vGAT, vGLUT1, and synapsin I puncta after Bin1 KD (Figure 2A). vGAT density was significantly impacted, decreasing by 17% following treatment with either shBin1^{1} or shBin1^{2} (Figure 2B). However, Bin1 KD did not affect vGLUT1 density (Figure 2C). The decrease in inhibitory synapses affected the overall presynaptic density, as indicated by a 13% and 23% reduction in synapsin I density, after treatment with shBin1^{1} and shBin1^{2}, respectively (Figure 2D). However, the postsynaptic density remained unaffected, as shown by the maintenance of gephrin density (Figures S2I and S2J). These results indicate that Bin1 regulates the number of inhibitory but not excitatory presynapses. To confirm these observations, we assessed the levels of vGAT, vGLUT1, and synapsin I after Bin1 KD (Figures 2E and S2K). We observed a 33% reduction in vGAT levels due to Bin1 KD (Figure 2F). Differently, the levels of vGLUT1 and synapsin I remained unchanged (Figures 2F and S2L). We confirmed that shBin1 reduced neuronal Bin1 (Figures 2G and 2H). Further analysis of synaptosomes obtained from primary neurons revealed a decrease in synapsin I in the SV fraction but not in the crude synaptosomal fraction (P2) (Figure 2I), indicating a loss of a subset of synapsin I-positive synapses upon Bin1 KD (Figure 2J). These data suggest that the loss of Bin1 function has a more significant impact on inhibitory synapses.

Next, we evaluated if the reduction in GABAergic synapses depends on the increased intracellular Aβ42 levels induced by Bin1 KD[26,27] since Aβ42 has been implicated in the loss of inhibitory synapses.[6,19] We treated neurons after Bin1 KD with BACE1 inhibitor (BACEi) and the γ-secretase inhibitor (N-[N-(3,5-difluorophenacetyl)-l-alanyl]-s-phenylglycinet-butylester, DAPT) as previously (Figure 2K). We confirmed that reducing Bin1 decreased the density of vGAT puncta by 41% (Figure 2L). However, treatment with DAPT and BACEi did not reverse the reduction in vGAT density (Figure 2L), size, or intensity (Figures S2M and S2N). These findings suggest that Bin1 plays a role in inhibitory synapses independent of Aβ production.

LOAD mutations in Bin1 cause loss of function in inhibitory synapses

Previously, we established that two coding variants in *BIN1* (rs754834233, P318L [Bin1^{PL}]; rs138047593, K358R [Bin1^{KR}]) associated with LOAD affect Bin1 function in controlling BACE1 endocytic recycling.[27] Thus, we hypothesized that Bin1 synaptic function would also be affected. To investigate whether Bin1 mutations interfere with Bin1 localization, expression, neuronal differentiation, and excitatory or inhibitory synapses, we compared Bin1^{PL} and Bin1^{KR} overexpression (OE) with Bin1 wild-type (Bin1^{WT}) or an MYC-empty vector (control) in neurons (Figure 3). We observed that the expression of Bin1^{PL} and Bin1^{KR} was similar to that of Bin1^{WT} (Figures 3A and 3B). The expression of Bin1 wild-type or mutants compared to the control (myc-vector) did not alter neuronal differentiation (Figures S3A and S3B).

To evaluate the impact of Bin1 mutations on synaptic localization, we compared the colocalization of Bin1^{WT}, Bin1^{PL}, and Bin1^{KR} with vGAT and vGLUT1 (Figures 3C and 3D). We noticed that Bin1^{WT}, Bin1^{PL}, and Bin1^{KR} concentrated in puncta resembling presynaptic boutons along the axon (Figures 3C and 3D). Interestingly, while 30% of Bin1^{WT} colocalized with vGAT, the Bin1^{KR} colocalized less with vGAT (Figures 3E and S3C). There was no difference in Bin1 colocalization with vGLUT1 (Figures 3F and S3D). These results suggest that the KR mutation interferes with Bin1 localization to GABAergic synapses.

To determine the impact of Bin1 WT and mutants' OE on synapses, we analyzed the density of vGAT, vGLUT1, and synapsin I puncta in axons (Figures 3G–3I and S3E). In contrast to Bin1 KD, Bin1^{WT} OE increased the density of vGAT puncta by 30%, emphasizing Bin1's critical role in inhibitory synapses (Figure 3H). In contrast, Bin1^{PL} and Bin1^{KR} did not increase the density of vGAT, suggesting that both mutations are deleterious (Figure 3H). In contrast, the density of vGLUT1 (Figure 3J) or synapsin I (Figure S3F) changes due to the OE of Bin1^{WT} and Bin1 mutants was undetectable, indicating that Bin1 is more relevant in inhibitory synapses.

To assess the capacity of Bin1^{WT} and mutants to rescue the reduction in vGAT puncta caused by Bin1 KD, we re-expressed them in neurons treated with shBin1 (Figure 3K). We confirmed that the density of vGAT decreased by 19% following Bin1 KD and that re-expressing Bin1^{WT} rescued vGAT density to control levels (Figure 3L), providing further evidence that Bin1 is a key component of inhibitory presynapses. Interestingly, the re-expression of Bin1 mutants failed to rescue the decreased vGAT density, with the effect of Bin1^{KR} being significantly different from that of Bin1^{WT}.

These results establish Bin1 as a critical component of inhibitory synapses. Mutations associated with LOAD appear to cause a loss of Bin1 function, affecting inhibitory synapses.

Bin1 KD causes neuron hyperexcitability

The loss of function of Bin1 may increase the activity of excitatory neurons by reducing the number of inhibitory synapses.

Figure 2. Bin1 KD reduces inhibitory synapses

Bin1 KD in neurons treated with shControl, shBin1^{1}, and shBin1^{2}, as indicated.

(A–D) Presynaptic density of vGAT, vGLUT1, and synapsin I. Scale bar, 5 μm (A). Density of vGAT (B), vGLUT1 (C), and synapsin I (D). n = 3–5; N = 28–168 axons; Mann-Whitney test vs. shControl (B) $^{*}p$ = 0.0399 shBin1^{1}, $^{**}p$ = 0.0079 shBin1^{2}; (D) $^{*}p$ = 0.0271 shBin1^{1}, $^{**}p$ = 0.0029 shBin1^{2}. ns, non-significant.

(E and F) vGAT, vGLUT1 levels normalized to GAPDH. n = 3; $^{**}p$ = 0.0064; ns, non-significant; paired t test.

(G and H) Bin1 levels normalized to tubulin. n = 3; $^{*}p$ = 0.0155; paired t test.

(I and J) Synapsin I levels in synaptosomal fractions: crude (P2), crude SVs (SV), and synaptosomal membrane (PSD). Bin1 immunoblot confirms KD (I) and quantification relative to shControl (J). Ho, homogenates. n = 3; $^{**}p$ = 0.0095 shControl$_{PSD}$ vs. shControl$_{SV}$, $^{*}p$ = 0.0316 shBin1$_{SV}$ vs. shControl$_{SV}$; ns, non-significant; repeated-measures one-way ANOVA.

(K and L) Effect of inhibiting beta-amyloid production with DAPT or BACEi on vGAT-positive synapses. Scale bar, 5 μm (K). Synaptic density (L). 3 independent experiments; n = 37–62 axons, $^{****}p < 0.0001$ vs. shControl$_{DMSO}$; ns, non-significant; Kruskal-Wallis test.

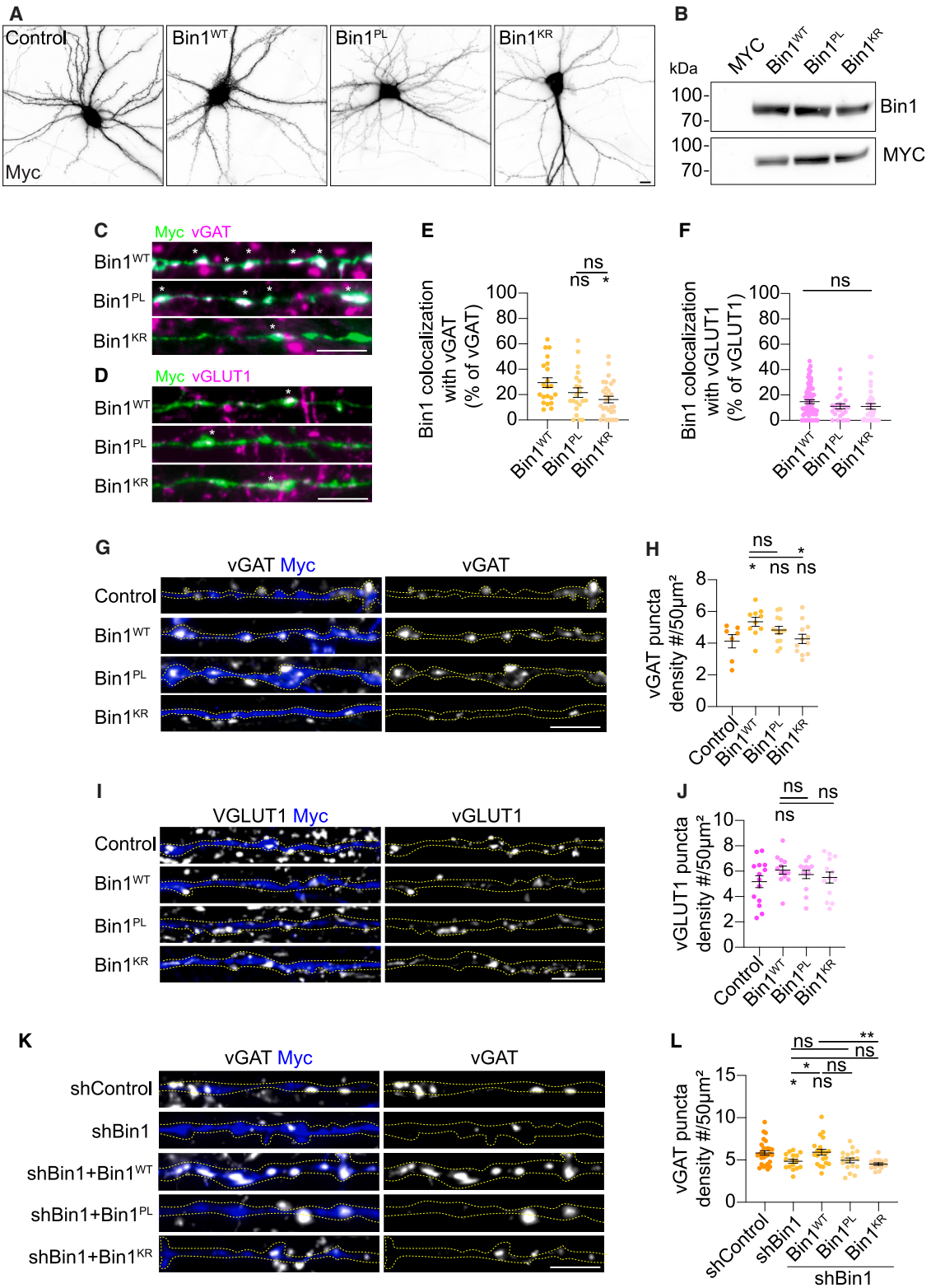

Figure 3. LOAD mutations in Bin1 cause loss of function in inhibitory synapses

Overexpression of MYC-tagged Bin1^{WT}, Bin1^{PL}, and Bin1^{KR}, and an empty vector expressing MYC (control) in 15 DIV neurons.
(A and B) Bin1^{WT}, Bin1^{PL}, Bin1^{KR}, and control immunofluorescence (Myc) (scale bar, 10 µm) (A) and expression levels in Neuro2a cells (B).

(legend continued on next page)

To test this hypothesis, we performed live imaging of multiple somatic calcium transients using Ca^{2+}-sensitive Fura Red dye (Figure 4A), adapted from.[39] We recorded the basal activity of shControl- and shBin1-treated neurons incubated with Fura Red in Tyrode solution (Figure 4B). Bin1 KD did not affect the % of active neurons showing calcium transients (Figure 4C). We noted that the baseline Fura Red mean fluorescence was higher in neurons treated with shBin1[1] (Figure 4D), indicating an imbalance in cytosolic calcium levels, which may be related to the impact of Bin1 on the trafficking of voltage-gated calcium channels.[33]

To evaluate the impact of inhibiting inhibitory synapses in control neurons, we added picrotoxin (PTX), a GABA receptor antagonist, after establishing the baseline. We observed a 39% increase in calcium transient frequency, from 4 to almost 6 spikes/min (Figure 4E), indicating increased neuronal activity compared to basal activity.[40] This increase likely reflects the activity of excitatory neurons, which are typically the most abundant in primary cortical cultures.[41] In neurons KD for Bin1, the calcium transient frequency was 7 spikes/min, similar to that of PTX-treated shControl neurons (Figure 4E), suggesting that Bin1 KD causes neuronal hyperexcitability. The application of PTX also increased spike amplitude by 56% in shControl neurons (Figure 4F) but not in shBin1 neurons (Figures S4A and S4B). The rise in calcium transient amplitude upon PTX but not in neurons treated with shBin1 indicates that postsynaptic activity is preserved upon Bin1 KD and not inhibited as upon PTX treatment.[42] Alternatively, the acute application of PTX does not fully replicate the effects of losing inhibitory synapses after 7 days of treatment with shBin1. Additionally, the Bin1-dependent loss of inhibitory synapses may lead to a homeostatic reduction in spike amplitude.[43]

To investigate whether an increase in glutamate release accompanies the increase in neuronal hyperexcitability, we monitored the fluorescence of the glutamate sensor iGluu, a postsynaptic sensor that increases fluorescence upon glutamate release (Figures S4C and S4G).[44] In neurons treated with shBin1, the glutamate release was 135% higher than in control neurons (Figures 4H and 4I). This finding aligns with the observed neuronal hyperexcitability. It suggests that, despite the noted reduction in vGLUT1-exocytosis, a higher content of glutamate per SV or exocytosis might occur at a greater frequency, leading to increased glutamate release.

We assessed the impact of Bin1 mutations on neuronal calcium levels by comparing the mean fluorescence of Fura Red in neuronal somas contacted by $Bin1^{PL}$- and $Bin1^{KR}$-expressing axons with those contacted by $Bin1^{WT}$ or control axons (Figure 4J). $Bin1^{PL}$ and $Bin1^{KR}$ increased the mean fluorescence of Fura Red compared to Bin1 wild type or the control (Figure 4K). This elevation in calcium levels aligns with the increased Fura Red fluorescence observed in Bin1 KD neurons (Figure 4D). These results show that LOAD mutations, PL and KR, result in loss of Bin1 function and, consequently, increased neuronal calcium levels, which could contribute to hyperexcitability.

An antiepileptic drug rescues Bin1 KD-dependent loss of inhibitory synapses and neuronal hyperexcitability

We identified levetiracetam (LEV), an antiepileptic drug that targets the presynaptic protein SV2, which binds to Bin1[45] and promotes GABAergic synaptic transmission. Interestingly, LEV treatment benefits the cognition of patients with AD.[46–49] We observed that SV2 colocalizes with Bin1 in perisomatic synapses (Figures 5A and 5B). Consistent with our hypothesis, LEV treatment increased the density of vGAT puncta by 31% in Bin1 KD neurons (Figures 5C and 5D). This increase occurred without affecting the density of vGAT in control neurons. Importantly, Bin1 KD alone led to a 45% decrease in vGAT density, validating our finding (Figure 3B).

Furthermore, we examined whether LEV could mitigate the neuronal hyperexcitability induced by Bin1 KD. We imaged live somatic calcium transients using Fura Red dye (Figure 5E) and, after recording the basal activity, added LEV to shBin1-treated neurons (Figure 5F). Bin1 KD neurons exhibited a significant increase in calcium transient frequency from 3 in control neurons to almost 5 spikes/min (Figures 5F and 5G), which confirms our previous findings (Figure 4E). Remarkably, LEV treatment partially reversed the hyperexcitability induced by Bin1 KD, reducing the calcium transient frequency to 4 spikes/min, corresponding to a 23% decrease (Figures 5F and 5G).

These results show that LEV effectively restores the loss of inhibitory synapses and mitigates neuronal hyperexcitability caused by Bin1 KD. These findings suggest that LEV may be an interesting therapeutic target for counteracting the loss of function of Bin1, thereby improving the number of GABAergic synapses and reducing hyperexcitability.

Bin1 is a regulator of the SV cycle via synaptic endosomes

Bin1 is an endocytic regulator that localizes to axonal early endosomes.[26] Endosomes/endosomal compartments are known to play a role in SV recycling in response to sustained stimulation.[50–53] Since Rab5 was found in SVs of rat hippocampal neurons,[54] we chose to study Bin1's impact on Rab5-positive early endosomes in presynaptic boutons (Figure 6). We detected Rab5-positive endosomes in synapsin I, vGLUT1, and vGAT puncta (Figures S5A and S5B), confirming Rab5 as a broad marker for presynaptic endosomes. Bin1 localized to synaptic endosomes, identified by Rab5 and synapsin I (Figure 6A). Through Imaris's super-resolution image reconstruction, we

(C–F) $Bin1^{WT}$, $Bin1^{PL}$, $Bin1^{KR}$ (Myc) colocalization with vGAT (C) or vGLUT1 (D). Scale bar, 5 μm; asterisk (*) indicates colocalization. Quantification of colocalization with vGAT (E) and vGlut1 (F). 3 independent experiments, n = 21–66, *p = 0.0222 $Bin1^{KR}$ vs. $Bin1^{WT}$; ns, non-significant; Kruskal-Wallis test.
(G–J) $Bin1^{WT}$, $Bin1^{PL}$, $Bin1^{KR}$ impact on presynaptic density. vGAT (G) or vGLUT1 (I) and Myc. Scale bar, 5 μm. Quantification of vGAT (H) and vGlut1 (J) density. 3 independent experiments; n = 7–14 axons, *p = 0.0233 $Bin1^{WT}$ vs. control; ns, non-significant; unpaired t test.
(K and L) Impact of $Bin1^{WT}$, $Bin1^{PL}$, and $Bin1^{KR}$ re-expression on vGAT density in Bin1 KD neurons. vGAT (gray) and Myc (blue). Scale bar, 5 μm. (K) Quantification of vGAT density (L). 3 independent experiments; n = 16–28, *p = 0.0199 shBin1 vs. shControl, *p = 0.0193 shBin1 vs. shBin1+$Bin1^{WT}$, ** p = 0.0096 shBin1+$Bin1^{WT}$ vs. shBin1+$Bin1^{KR}$; ns, non-significant; Mann-Whitney test.

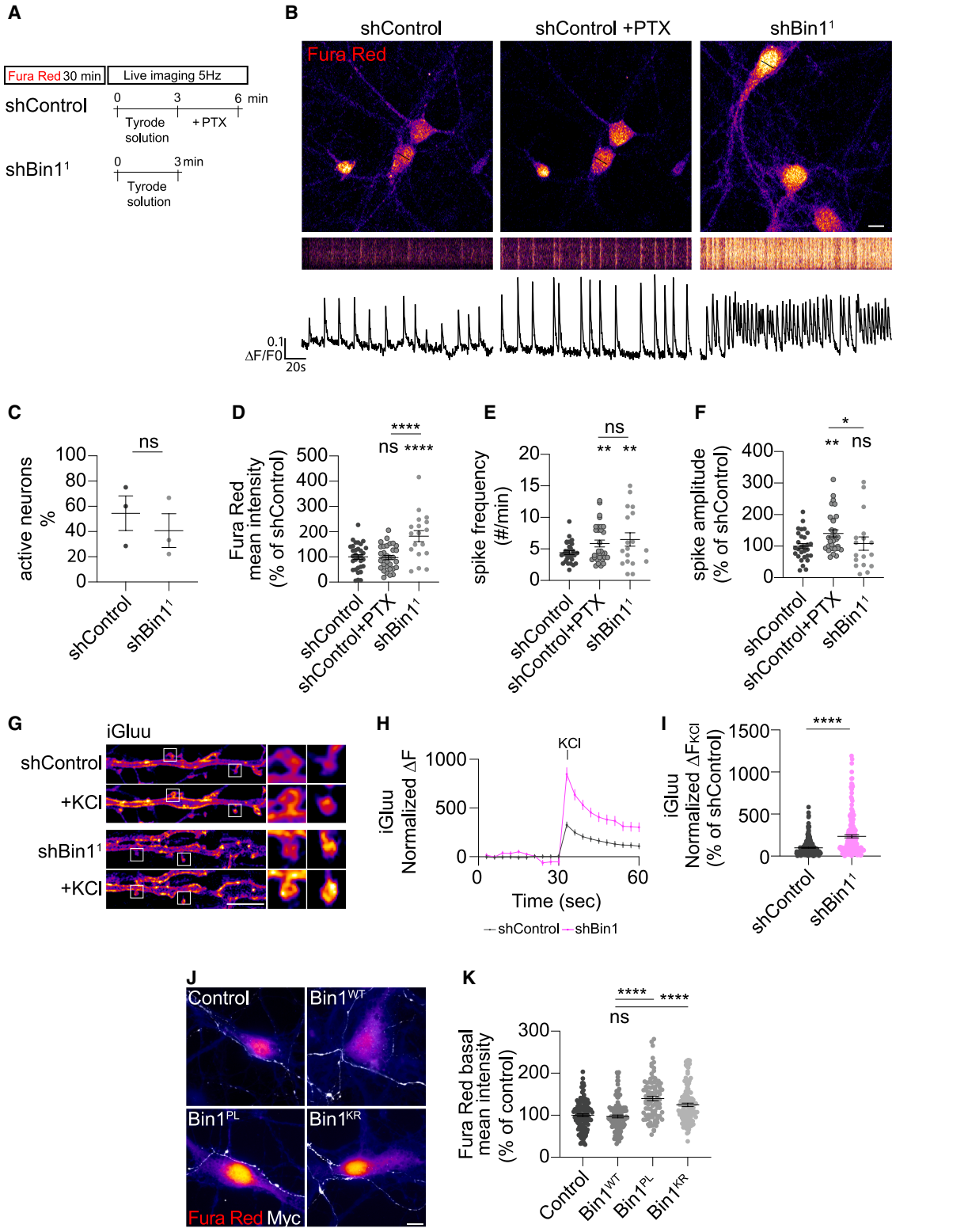

Figure 4. Bin1 KD increases neuronal network excitability

(A–F) Calcium imaging using Fura Red. Protocol schematics (A). Fura Red (Fire LUT) in shControl neurons after 30-min incubation and after 3 min with Picrotoxin (PTX) and shBin1[1] neurons (scale bar, 10 μm). Black lines over the neuronal somas were used to generate kymographs of the time series. The corresponding representative traces of Fura Red (ΔF/F0) are below. Quantification of the percentage of active neurons (C), Fura Red mean intensity (D), spike frequency (E), and

(legend continued on next page)

discerned Bin1 juxtaposed to a Rab5-positive endosome within a synapsin I-positive presynaptic bouton (Figure 6B).

Previously, we found that loss of function of Bin1 by KD or mutations enlarged early endosomes.[26,27] However, early endosomes were smaller in neurons knockout for Bin1.[33] To assess the impact of Bin1 KD on the presynaptic endosomes in excitatory and inhibitory synaptic boutons, we detected Rab5-positive endosomes in vGAT and vGLUT1 in shControl- and shBin1-treated neurons (Figure 6C). To analyze the frequency of smaller (0.03–0.1 μm^2) and larger (0.1–0.5 μm^2) puncta, we used sequential segmentation of the synaptic marker and Rab5 and extracted the size of each synaptic Rab5 punctum (Figure 6A). In neurons treated with shControl, Rab5-positive endosomes were distributed in 58% smaller and 42% larger endosomes in vGAT synapses (Figure 6D). In neurons treated with shBin1, Rab5-positive endosomes were distributed in 71% smaller and 39% larger endosomes in vGAT synapses. In synapses with vGLUT1, the smaller Rab5-positive endosomes made up a larger proportion (67%), and there was no difference in endosome size distribution when Bin1 was KD. The results indicate that reducing Bin1 decreased the size of inhibitory synaptic endosomes. This appears to be a localized effect, as Bin1 KD did not influence the Rab5 levels measured by western blot (Figures S5C and S5D) or immunofluorescence in mature neurons (Figure S5E).

Similarly, we assessed whether $Bin1^{WT}$ or mutants impacted the size of Rab5-positive endosomes in synapsin I-positive synapses. In control cells, Rab5 puncta were distributed in 53% smaller and 47% larger endosomes (Figures 6E and 6F). This distribution remained unchanged with both $Bin1^{WT}$ and $Bin1^{PL}$ OE. However, OE of $Bin1^{KR}$ caused a shift to smaller endosomes (58%), like Bin1 loss, indicating that the KR mutation affects Bin1's function in inhibitory synaptic endosomes.

These results suggest that Bin1 regulates larger endosomes at inhibitory synapses but not at excitatory ones. Supporting evidence suggests that GABAergic synapses preferentially utilize large endosomes to regenerate SVs. The KR mutation in Bin1 associated with LOAD disrupts this function.

To gain deeper insight, we investigated Bin1's role in SV exocytosis and endocytosis by stimulating shBin1-treated synaptic boutons in the presence of the FM4-64FX dye. We detected active individual presynaptic boutons at steady state by the uptake of FM4-64FX after 90 s of high K^+ depolarization, allowing SV to be released and FM4-64FX to be loaded upon compensatory endocytosis (Figure 6G). After washing with Tyrode solution containing tetrodotoxin (TTX), neurons were fixed. FM-loaded active synaptic puncta, size, and mean intensity were measured proximal to the soma and distally (Figure 6H). Bin1 KD reduced FM puncta's density, size, and intensity in the perisomatic region but not distally, where only the FM puncta's mean intensity tended to decrease (Figures 6I–6K). The decrease in perisomatic puncta suggests that Bin1 KD reduces the active axo-somatic synapses, which are primarily inhibitory.[55]

Next, we imaged FM4-64FX-labeled synapses in live neurons after stimulation with high K^+ depolarization (load) and after a second K^+ depolarization to stimulate the exocytosis (unload) of the newly reformed SV labeled by endocytosis during the first stimulation (Figure S5F). We observed active synapses brightly labeled with FM4-64FX upon stimulation (load) (Figure S5G). Since no cell bodies were detected in the videos, we speculate that most labeled synapses were distal excitatory. The FM-loaded puncta mean intensity was decreased in shBin1-treated neurons (Figure S5H), indicating that detection of FM labeling in live neurons is more sensitive than in the fixed neurons since distal synapse labeling only tended to decrease in the latter. Bin1 KD reduced the uptake of the FM dye, consistent with Bin1 regulating excitatory SV endocytosis. During unloading, FM fluorescence decreased from 2 to 60 s, consistent with SV exocytosis (Figure S5I). In neurons treated with shControl, the mean intensity of FM-loaded puncta was reduced by 22% and 31% after 2 and 60 s, respectively (Figure S5I). In contrast, in neurons treated with shBin1, the mean intensity of FM-loaded puncta remained unchanged after 2 s. Although fluorescence decreased after 60 s, it was still higher than the control (Figure S5I). Bin1 KD reduced the release of SV labeled with FM dye, consistent with Bin1 regulating excitatory SV exocytosis.

These results suggest that Bin1 plays a crucial role in inhibitory synapses compared to excitatory ones, as Bin1 KD reduces activity in both types but only impacts the density of inhibitory synapses.

Bin1 differentially regulates the GABAergic and glutamatergic SV cycle

To understand the distinct roles of Bin1 in inhibitory GABAergic synapses and excitatory synapses, we investigated SV exocytosis and endocytosis in each type of synapse. We used vGAT-pHluorin under the GAD67 promoter to evaluate SV traffic in inhibitory neurons and vGLUT1-pHluorin under the CAMKIIα promoter for excitatory neurons (Figure 7A).[56] Following transfection with pHluorins (7 DIV), neurons were treated with shBin1 or shControl (11 DIV). Live neurons (15 DIV) were imaged in Tyrode solution for a baseline (30 s) and in a depolarizing solution to stimulate SV exocytosis and compensatory endocytosis (60 s). Finally, NH_4Cl was added to assess the total expression of pHluorins by alkalinizing both surface and internal pools (50 s) (Figure 7B). The variation in vGAT- or

amplitude (F). 3 independent experiments, n = 17–32 soma; (D) shBin1 vs.: ****$p < 0.0001$ shControl; ****$p > 0.0001$ $shControl_{PTX}$, unpaired t test; (E) vs. shControl: **$p = 0.0057$ $shControl_{PTX}$, **$p = 0.0095$ shBin1, (F) **$p = 0.0078$ $shControl_{PTX}$ vs. shControl, *$p = 0.0330$ $shControl_{PTX}$ vs. shBin1; ns, non-significant; Kruskal-Wallis test.

(G–I) Glutamate release with iGluu imaging in the axons of neurons treated with $shControl^1$ and $shBin1^1$. iGluu (Fire LUT) at baseline and after stimulation (high K^+). Scale bar, 5 μm (G). Quantification of iGluu fluorescence intensity (ΔF) over time (seconds) in shControl and shBin1 neurons (H) and immediately after high K^+ stimulation (ΔF_{KCl}) (I). 3 independent experiments, $n = 180–229$; ****$p < 0.0001$; Mann-Whitney test.

(J and K) Impact of presynaptic $Bin1^{WT}$, $Bin1^{PL}$, $Bin1^{KR}$, and control on postsynaptic calcium (Fura Red). $Bin1^{WT}$, $Bin1^{PL}$, $Bin1^{KR}$, and control (Myc, gray) and Fura Red (Fire LUT) (J) and quantification of Fura Red (Fire LUT) mean intensity (K). 3 independent experiments, n = 94–125 axons; vs. $Bin1^{WT}$, **** $p < 0.0001$ $Bin1^{PL}$, **** $p < 0.000$ $Bin1^{KR}$; ns, non-significant; Kruskal-Wallis test.

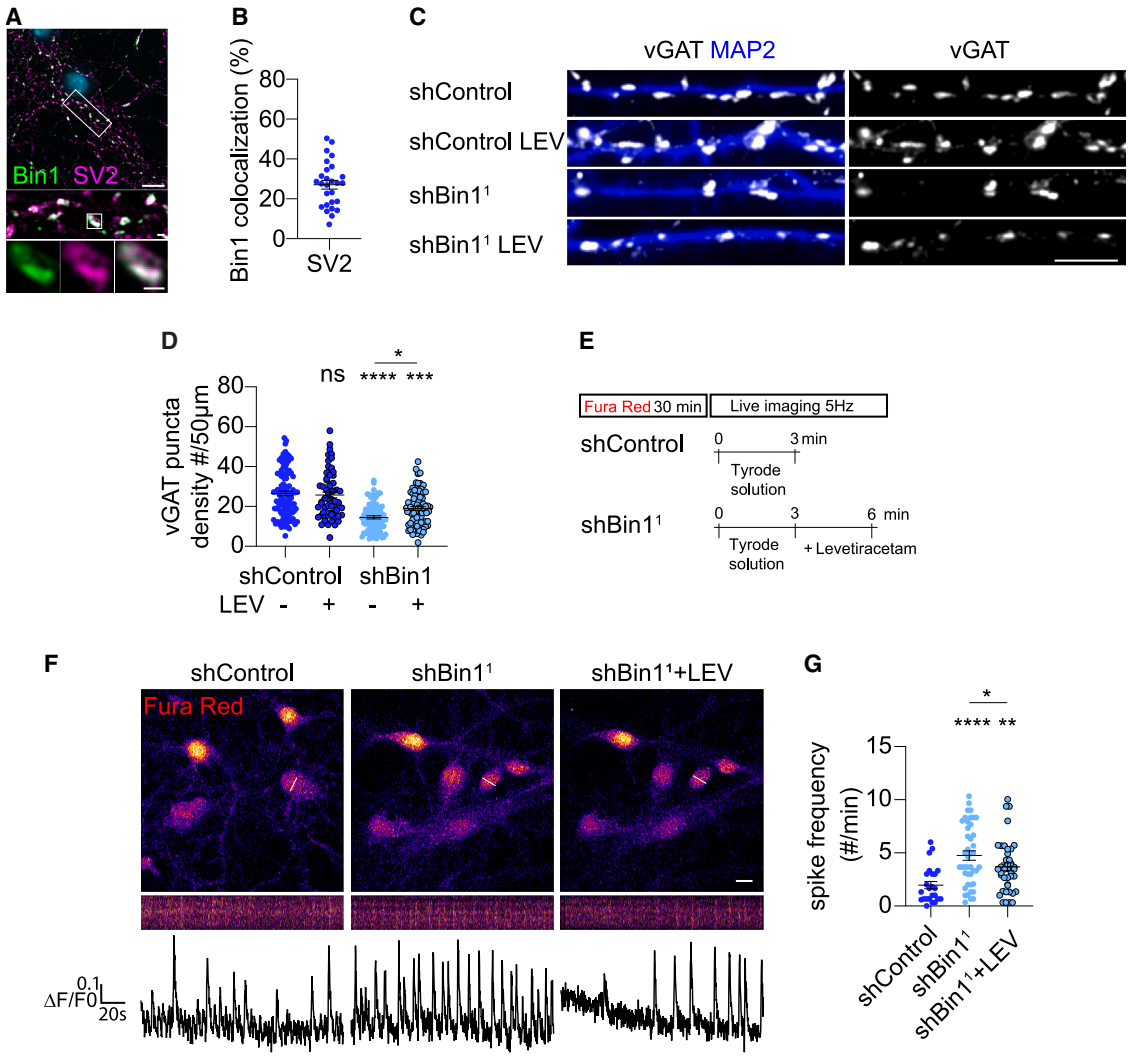

Figure 5. Levetiracetam rescues Bin1 KD-dependent neuronal hyperexcitability

(A and B) Bin1 colocalization with SV2. Scale bars, 10 µm, 1 µm (synaptic punctum). n = 3; N = 27 neurons.(C and D) Levetiracetam (Lev) treatment of vGAT synapses in neurons KD for Bin1. vGAT (gray) and MAP2 (blue) in shControl, shBin1^{1} neurons with or without LEV. Scale bar, 5 µm (C). Quantification of vGAT density (D). 3 independent experiments; n = 61–104 neurites; vs. shControl: ****p < 0.0001 shBin1, ***p = 0.0003; *p = 0.0175 shBin1 vs. shBin1$_{LEV}$; ns, non-significant; Mann-Whitney test.

(E–G) LEV impact on calcium transients. Protocol schematics (E). Fura Red (Fire LUT), in shControl and shBin1^{1} neurons, and shBin1^{1} after LEV (scale bar, 10 µm). White lines (neuronal somas) produced time-series kymographs. Below are representative traces of Fura Red (ΔF/F0). (F) Quantification of calcium spike frequency (G). 3 independent experiments; n = 26–43 soma; ***p = 0.0002 shBin1 vs. shControl, **p = 0.0027 shBin1$_{LEV}$ vs. shControl, Mann-Whitney test, *p = 0.0263 shBin1$_{LEV}$ vs. shBin1; Wilcoxon test.

vGLUT1-pHluorin fluorescence in individual boutons relative to baseline (ΔF) was normalized to total expression (F_{NH4Cl}) (Figures 7C and 7D).

At baseline, vGAT-pHluorin fluorescence was increased by 2-fold with Bin1 KD (Figures S5G and S5H), but vGLUT1-pHluorin was unaltered (Figures S5G and S5H), suggesting that vGAT levels at the plasma membrane are increased upon Bin1 KD. With stimulation, both vGAT- and vGLUT1-pHluorin fluorescence increased sharply due to exocytosis and plasma membrane exposure to the neutral pH of the live-imaging medium (Figures 7C and 7D), consistent with rapid SV release.[56] Subsequently, both vGAT- and vGLUT1-pHluorin fluorescence declined (Figures 7C–7H) due to endocytosis and reacidification. Finally, fluorescence sharply increased with NH_4Cl-dependent alkalinization (Figures 7C and 7D).

Upon the KD of Bin1 following stimulation, we observed a differential change in the exocytosis of vGAT-pHluorin and vGLUT1-pHluorin. Specifically, in Bin1 KD neurons, the peak in vGAT-pHluorin fluorescence was 43% higher than in control neurons (Figure 7F). Conversely, the peak fluorescence of vGLUT1-pHluorin was 40% lower in the Bin1 KD neurons compared to the control (Figure 7G). These findings suggest that Bin1 has distinct roles in regulating the release of inhibitory and excitatory SVs. Specifically, Bin1 may be a negative regulator of SV release

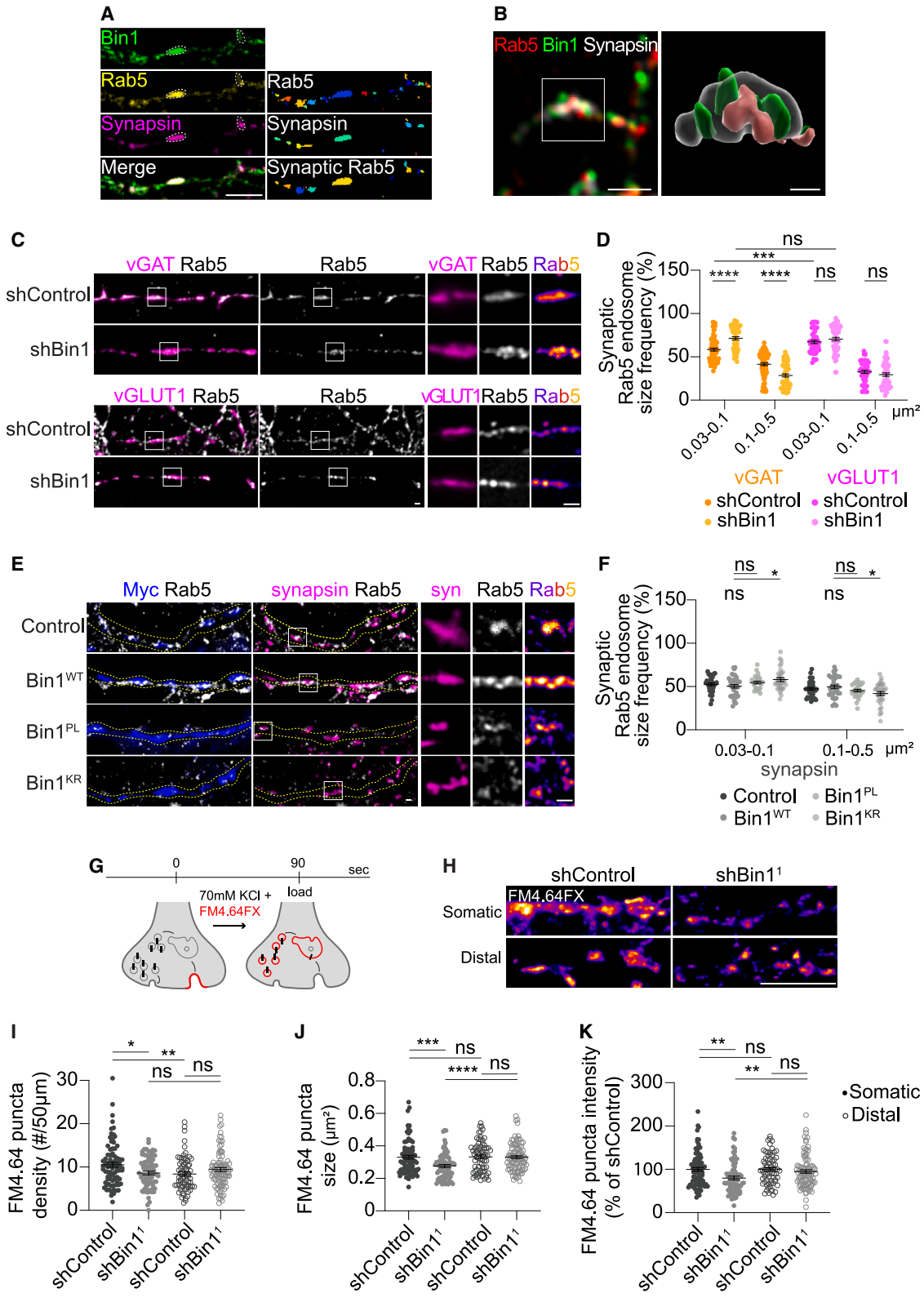

(legend on next page)

in inhibitory synapses and play a minor role as a positive modulator in excitatory synapses.

During recovery, the decline in vGAT-pHluorin fluorescence was remarkably faster in neurons treated with shBin1 (Figure 7H). The time constant for inhibitory SV endocytosis τ (s) in shBin1-treated neurons was 23% faster (15 s) than in control cells (20 s) (Figure 7I), suggesting an increase of SV endocytosis in inhibitory synapses. Conversely, Bin1 KD did not alter the decline of vGLUT1-pHluorin fluorescence (Figure 7J), suggesting that Bin1 does not regulate SV endocytosis in excitatory synapses.

To assess whether the impact of Bin1 KD on vGAT-SV exocytosis was accompanied by increased GABA release, we expressed a GABA fluorescent sensor, iGABASnFR2,[57] in neurons treated with shBin1 (Figures 7K and S4C). This postsynaptic sensor increases fluorescence upon high potassium-evoked GABA release. We detected a 146% increase in iGABASnFR2-normalized fluorescence in Bin1 KD neurons compared to control neurons (Figures 7L and 7M), supporting that Bin1 KD neurons release more GABA.

Our results suggest that Bin1 is an inhibitor of SV exocytosis and endocytosis in GABAergic synapses but an activator of SV exocytosis in glutamatergic synapses. Bin1, required for excitatory SV release, correlates with the decrease in the unloading of FM-labeled SV, likely from excitatory synapses, and this finding aligns with previous results showing presynaptic excitatory SV accumulation when Bin1 is KD in glutamatergic synapses.[32] It is surprising and intriguing that Bin1 opposes the inhibitory SV cycle. Future research should clarify how Bin1 regulates the SV cycle, identify a possible regulatory loop, or determine whether this increased inhibitory SV cycle is a compensatory response to the loss of inhibitory synapses.

In LOAD, Bin1 loss of function may dysregulate the SV cycle, eliminating inhibitory synapses and consequently contributing to glutamatergic hyperexcitability.

DISCUSSION

We set out to investigate the role of endosomal Bin1 in synapses and its disruption by LOAD risk mutations, which may be relevant to the development of AD.

We discovered a physiological function for Bin1 in inhibitory synapses. We demonstrate that LOAD risk mutations primarily disrupt Bin1 function in inhibitory synapses, where Bin1 associates with synaptic endosomes to regulate the SV cycle independently of amyloidogenesis. The Bin1-dependent loss of inhibitory synapses leads to neuronal hyperexcitability, which may underlie the appearance of seizures early in patients with LOAD. Importantly, treatment with levetiracetam, an antiepileptic drug, showed potential in decreasing the Bin1-dependent loss of inhibitory synapses and hyperexcitability.

Overall, we identified a mechanism for inhibitory synapse loss with therapeutic potential for preventing or treating seizures and delaying disease onset in patients with the Bin1 risk genotype.

Bin1 critical function in inhibitory synapses

We established that Bin1 increases with synaptic maturation and in response to synaptic activity. However, unlike synapsin I, Bin1 is enriched in a subset of synapses in the perisomatic region, consistent with axo-somatic inhibitory synapses.[55] Indeed, Bin1 was more abundant in inhibitory synapses, identified by the GABA transporter vGAT, than in excitatory synapses, identified by vGLUT1, in both cultured and brain neurons. This finding is supported by a higher correlation of Bin1 with inhibitory synapses revealed by proteomics of fluorescence-activated synaptosome sorting,[58] along with gene expression data (Human Protein Atlas),[59] despite earlier analysis revealing a similar proteome in inhibitory and excitatory SVs.[60]

We found that inhibitory synapses require Bin1. vGAT-positive, but not vGLUT1-positive, synaptic boutons are lost upon Bin1 KD, increased upon Bin1 OE, and rescued by the re-expression of Bin1 in Bin1-depleted neurons. Possibly linked to the loss of inhibitory synapses, the cellular levels of vGAT, but not vGLUT1, were decreased in neurons KD for Bin1, which can relate to vGAT degradation upon removal from synapses.[61] FM-labeled active perisomatic synapses (mostly inhibitory), but not distal ones (mostly excitatory), were reduced in Bin1 KD. Interestingly, we also found a decrease in FM unloading at active distal synapses, consistent with previously identified defects in excitatory synapses.[32,36]

Bin1 function in the SV cycle

We discovered that Bin1 functions differently in inhibitory and excitatory synapses. Bin1 negatively regulates inhibitory SV exocytosis and GABA release while positively regulating excitatory SV exocytosis. Moreover, Bin1 negatively regulates inhibitory but not excitatory SV endocytosis.

There are still scarce studies on the SV cycle in inhibitory synapses. The increase in inhibitory SV exocytosis by Bin1 KD could result from decreased SV tethering,[62] since synapsin I was less associated with SV synaptosomal fraction, and synapsin I

Figure 6. Bin1 loss of function reduces the size of presynaptic endosomes

(A) Bin1 colocalization with Rab5 in synapsin I-positive puncta (outlined). Scale bar, 5 μm. The right panels exemplify sequential segmentation of synaptic Rab5 for (D).

(B) Super-resolution image of a synaptic punctum identified by synapsin I with Bin1 and an endosome labeled by Rab5. Imaris 3D reconstruction. Scale bar, 0.3 μm.

(C–F) Impact of Bin1 KD or overexpression of Bin1 wild type and mutants on synaptic endosomes. Rab5-positive endosomes in vGAT-positive or vGLUT1-positive synapses in neurons treated with shControl or shBin1 (C) or in synapsin I-positive synapses in neurons expressing $Bin1^{WT}$, $Bin1^{PL}$, $Bin1^{KR}$, and control (E). White squares highlight magnified synaptic endosomes. Scale bars, 1 μm. Quantification of the frequency of small (0.03–0.1 μm^2) or large (0.1–0.5 μm^2) endosomes (D and F). (D) 3 independent experiments; n = 46–75 neurites; $^{****}p < 0.0001$ $shBin1_{vGAT}$ vs. $shControl_{vGAT}$, $^{***}p = 0.0010$ $shControl_{vGAT}$ vs. $shControl_{vGLUT1}$ (0.03–0.1); Mann-Whitney test. (F) $n = 3$, $N = 36$ axons; $^{*}p = 0.0124$ $Bin1^{WT}$ vs. $Bin1^{KR}$; ns, non-significant; unpaired t test.

(G–K) FM4.64FX uptake upon stimulation in somatic and distal neurites of neurons treated with shControl and $shBin1^{1}$. Scale bar, 10 μm (H). Quantification of FM4.64 puncta density (I), size (J), and mean intensity (K). 3 independent experiments, $n = 70–93$ neurites. (I) $^{*}p = 0.0319$ vs. $shBin1_{somatic}$ vs. $shControl_{somatic}$ $^{**}p = 0.0057$ $shControl_{distal}$ vs. $shControl_{somatic}$. (J) $^{***}p = 0.0006$ $shBin1_{somatic}$ vs. $shControl_{somatic}$, $^{****}p < 0.0001$ $shBin1_{somatic}$ vs. $shBin1_{distal}$. (K) $^{**}p = 0.0013$ $shBin1_{somatic}$ vs. $shControl_{somatic}$; ns, non-significant; Mann-Whitney test.

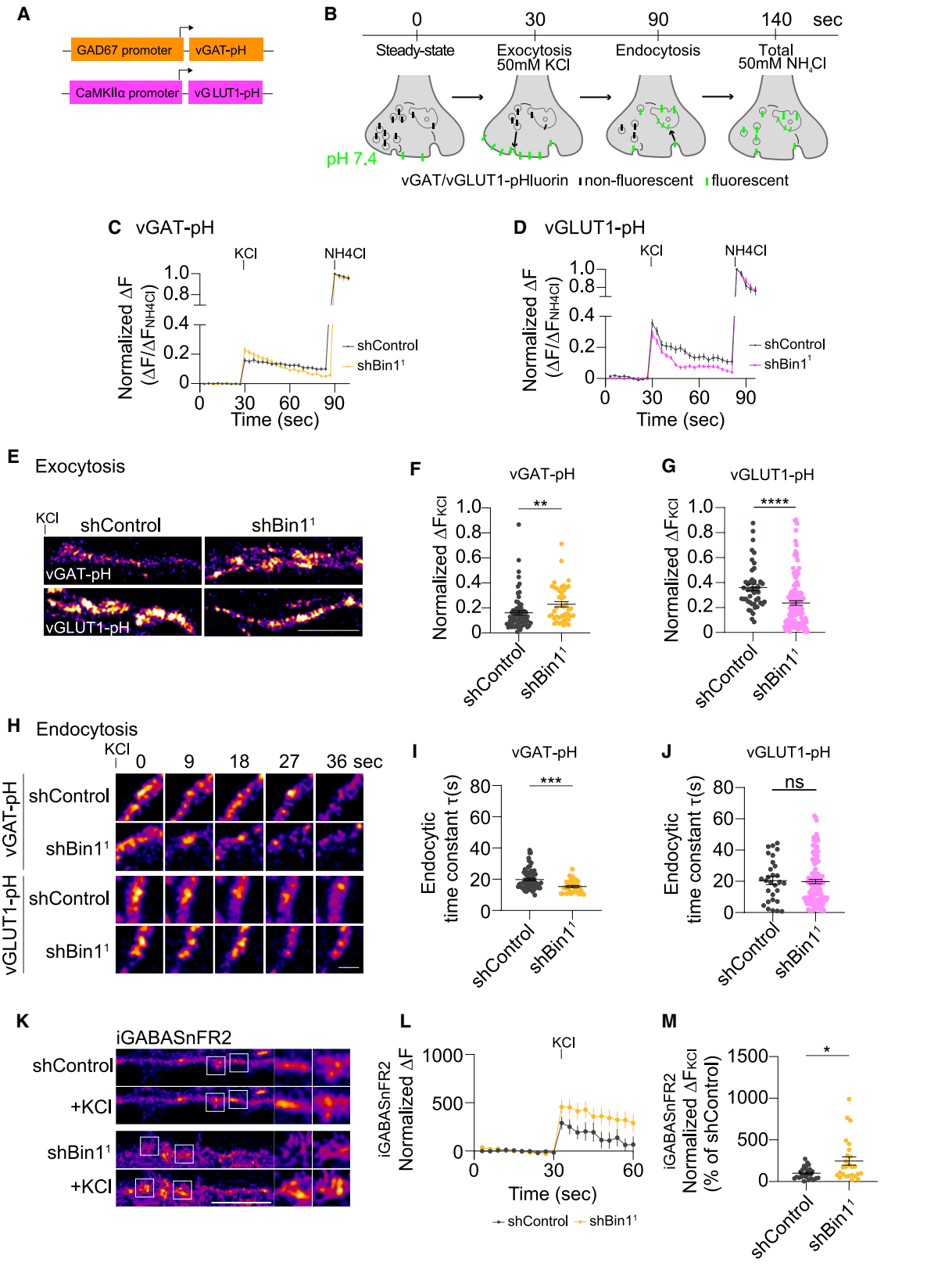

(legend on next page)

maintains the readily releasable SV pool (RRP) of GABAergic synapses.[63,64] Alternatively, it could also result from the higher rate of compensatory endocytosis and a consequent larger RRP. Interestingly, vGAT exocytosis was described to increase, as in Bin1 KD, when it interacts with clathrin adaptor protein AP-3 instead of AP-2[65], suggesting that a lack of Bin1 could promote vGAT interaction with AP-3 and inhibitory SV release. Also, our findings are consistent with the decreased SV release observed in human glutamatergic neurons knocked out for Bin1,[32] which could be related to the reduced scission of SVs off synaptic endosomes, as seen with BACE1.[26]

Remarkably, the Bin1 KD-induced acceleration of vGAT endocytosis aligns with the proposed role of Bin1 as a negative regulator of endocytosis.[66] The hypothesis involves Rab5 overactivation. Interestingly, Bin1 interacts with RIN3, a Rab5 activator (GEF),[67] which is also associated with LOAD risk and, thus, a potential mechanistic target for future research. Rab5, found in early endosomes and on synapses,[54] is proposed to help maintain SV size by preventing homotypic fusion.[68] We demonstrate that Bin1 KD decreases the size of GABAergic, but not glutamatergic, presynaptic endosomes in mature neurons. In contrast, canonical early endosomes are enlarged in immature neurons upon Bin1 KD.[26] There could be a distinct set of regulatory partners of Bin1 in canonical and synaptic early endosomes or changes in the endosomal system with neuronal maturation. In canonical early endosomes, the enlargement was due to reduced scission of recycling intermediates and cargo accumulation. In contrast, inhibitory synaptic endosomes became smaller in the absence of Bin1, likely due to the acceleration of SV recycling/exocytosis. Inhibitory synaptic endosomes may be more dependent on Bin1 than excitatory ones, which can rely on alternative SV endocytic pathways, as proposed.[69]

We concluded that Bin1, although involved in the function of excitatory synapses, plays a less critical role, mainly because the reduction in excitatory SV exocytosis by Bin1 KD was insufficient to alter the density of vGLUT1 synapses. Otherwise, the loss of Bin1 reduced inhibitory synapses, and the remaining ones exhibited faster SV endocytic recycling. This could lead to the depletion of the synaptic endosome and, ultimately, the exhaustion and elimination of inhibitory synapses.

Bin1 loss of function is relevant for AD

Aβ aggregation has been implicated in inhibitory and excitatory synapse loss.[11,70] Thus, we hypothesized that the increased Aβ production we observed upon Bin1 KD could trigger the loss of inhibitory synapses. Unexpectedly, our results do not support this hypothesis as vGAT synapse loss upon Bin1 KD was not protected by inhibiting γ-secretase or BACE1. In the same experimental conditions, inhibition of Aβ production rescued aging-dependent synaptic decline[71] and CD2AP LOAD risk gene KD-dependent spine loss.[72] Our findings suggest that the loss of Bin1 function may disrupt synapses before Aβ accumulation, potentially due to aging, resulting in synapse dysfunction. Importantly, we discovered that the two LOAD risk-coding variants in *BIN1*, the PL and the KR mutations, cause loss of function in Bin1 at inhibitory synapses. $Bin1^{PL}$ or $Bin1^{KR}$ could not revert the vGAT-positive synapse loss caused by Bin1 KD or increase vGAT synapse density when overexpressed. The KR mutation had a dominant-negative effect on inhibitory synaptic endosome size and the $Bin1^{WT}$-induced increase in vGAT density. These results, along with our previous findings on amyloidogenesis, support that the KR mutation is more pathogenic than the PL. Interestingly, the KR mutation in a familial AD mouse model aggravated amyloid pathology and influenced synapse density and plasticity.[73]

We found that, while the mutations do not interfere with Bin1 exogenous expression, the Bin1 KR mutant reduces Bin1 localization to GABAergic synapses. Both mutations may disrupt Bin1 self-inhibition by interfering with intramolecular CLAP-SH3 binding.[74] The KR mutation, in the SH3 domain, may hinder Bin1 interactions with SV recycling proteins, such as dynamin, AP-2, and synaptojanin.[75–77] Future work should assess how the LOAD mutations impact Bin1's function in the SV cycle to implicate further Bin1's role in the synaptic dysfunction in LOAD.

Bin1 loss of function may be a cause for seizures early in LOAD

Functional imaging shows early hyperactivation in AD patients,[78–81] suggesting neuronal hyperexcitability precedes later hypoactivity. We propose that Bin1 loss of function contributes to this hyperexcitability independently of Aβ or APOE4. Bin1 KD increases glutamate release and spontaneous calcium transients, mimicking the effect of inhibitory blockade. This likely reflects a reduction in inhibitory synapse function, leading to the disinhibition of excitatory neurons. Bin1 KD or LOAD variants also elevate basal calcium levels, potentially via impaired Cav1.2 trafficking. Supporting this, inhibitory synapse loss is observed in AD brains,[19] and interneuron dysfunction is reported in AD mouse models.[70,82] Furthermore, Bin1 dysfunction is implicated in stiff person syndrome, where amphiphysin autoantibodies target a Bin1 homolog,[83] and Bin1 OE in mice also causes network hyperexcitability,[37] underscoring the need for its tight regulation.

Figure 7. Bin1 differentially regulates GABAergic and glutamatergic SV cycle

(A–J) Bin1 KD impact on vGAT/vGLUT1-pH. vGAT/vGLUT1-pH plasmids (A) and illustration of pHluorins protocol (B). vGAT/vGLUT1-pH fluoresce at pH 7.4 (steady state; 30 s), after stimulation (60 s), and after the addition of NH_4Cl (50 s). Fluorescence intensity ($\Delta F/\Delta F_{NH4Cl}$) of vGAT-pH (C) and vGLUT1-pH (D) in neurons treated with shControl (black) and shBin1 (yellow/magenta). 3 independent experiments, n = 45–133. Axonal vGAT-pH and vGLUT1-pH (Fire LUT) fluorescence immediately after high K^+. Scale bar, 5 μm (E), and the subsequent fluorescence decay. Scale bar, 1 μm (H). Quantification of fluorescence ($\Delta F_{KCl}/\Delta F_{NH4Cl}$) of vGAT-pH (F) and vGLUT1-pH (G) and the endocytic time constant (t) of vGAT-pH (I) and vGLUT1-pH (J). (F) $^{**}p = 0.0018$. (G) $^{****}p < 0.0001$. (I) $^{***}p = 0.0004$ shControl vs. shBin1. (J) $^{ns}p = 07232$; ns, non-significant; Mann-Whitney test.

(K–M) GABA release with iGABASnFR2 imaging in the axons of neurons treated with shControl[1] and shBin1[1] at baseline and after stimulation (high K^+). Scale bar, 5 μm. White rectangles indicate magnified punctum (scale bar, 0.5 μm) (K). Quantification of iGABASnFR2 fluorescence intensity (ΔF) over time (seconds) in shControl (black) and shBin1 (yellow) neurons (L) and ΔF_{KCl} (M). 3 independent experiments, n = 27–39 puncta. (L)$^{*}p = 0.0122$; Mann-Whitney test.

Importantly, the antiepileptic levetiracetam reduced both vGAT synapse loss and restored calcium transients altered by Bin1 KD. Moreover, we found that SV2, the target of levetiracetam, colocalizes with Bin1. This result may explain why LEV treatment reduced hippocampal activation in patients with mild-cognitive impairment (MCI) and improved cognitive function.[84] Future research should assess inhibitory transmission in mice, particularly Bin1 KD in inhibitory neurons, and focus on MCI/AD patients with seizures or hyperactivation related to the *BIN1* risk genotype. The potential of antiepileptic drugs for individuals with LOAD carrying the Bin1 risk genotype should be evaluated.

We have identified a role for Bin1 in inhibitory synapses, where it regulates both SV exocytosis and endocytosis. This regulation likely affects synaptic transmission and, ultimately, memory. We demonstrate that LOAD mutations lead to loss of function of Bin1. Bin1 KD triggered hyperexcitability due to Bin1-dependent deregulation of inhibitory synapses, which could be linked to hyperactivation in patients with LOAD, through mechanisms independent of Aβ. LOAD genetic variations in *BIN1* may drive these disturbances and might need to be addressed therapeutically before anti-amyloid treatments.

Overall, we identified a mechanism for inhibitory synapse loss with therapeutic potential for preventing or treating seizures and delaying disease onset in patients with the *BIN1* risk genotype.

Limitations of the study

The study's limitations include its primary reliance on mouse models, which require validation in humans. It identifies a link between Bin1 loss and accelerated SV cycle in inhibitory neurons and reduced SV exocytosis in excitatory neurons; however, the precise molecular mechanisms need further investigation. Future studies should include non-coding variants in *BIN1* and patient-derived neurons to confirm hyperactivation in patients with the *BIN1* risk genotype and the efficacy of levetiracetam through preclinical and clinical trials.

RESOURCE AVAILABILITY

Lead contact

Further information and requests should be directed to the lead contact, Cláudia Guimas Almeida (claudia.almeida@nms.unl.pt).

Materials availability

This study did not generate new unique reagents.

Data code and availability

- All data supporting this study's findings are available either within the paper or from the lead contact upon request.
- This paper does not present original code.
- The lead contact can provide any additional information required to re-analyze the data reported in this paper upon request.

ACKNOWLEDGMENTS

We thank the lab members for their helpful discussions and critical review of the manuscript. We thank Dr. S. Marques and Dr. T. Pereira (NMS Platforms). This study received funding (to C.G.A.) from the Research Unit UID/04462: iNOVA4Health-Programa de Medicina Translacional and the Associated Laboratory LS4FUTURE (LA/P/0087/2020), all financially supported by Fundação para a Ciência e a Tecnologia (FCT)/Ministério da Educação, Ciência, e Tecnologia and co-funded by FEDER under the PT2020 Partnership Agreement (Portugal), Maratona da Saúde 2016, and the research infrastructure PPBI-POCI-01-0145-FEDER-022122 (FCT and Lisboa2020, under the PORTUGAL2020 agreement - European Regional Development Fund); to E. R.G., from the European Research Council(H2020GA 810207-ARPCOMPLEXITY). C.G.A. has been supported by FCT (CEECIND/00410/2017, CEEC/iNOVA4Health). C.P. and M.A.B. received an FCT doctoral fellowship (PD/BD/128374/2017; https://doi.org/10.54499/2020.06758.BD).

AUTHOR CONTRIBUTIONS

Conceptualization, C.G.A., C.P., and M.A.B.; methodology, C.G.A., C.P., M.A.B., and J.R.; formal analysis, M.A.B., C.P., and C.G.A.; investigation, M.A.B., C.P., C.G.A., and J.R.; writing – original draft, C.P. and M.A.B.; writing, M.A.B., C.G.A., C.P., J.R., and E.R.G.; visualization, M.A.B., C.P., and C.G.A.; supervision, C.G.A. and E.R.G.; project administration, C.G.A.; funding acquisition, C.G.A. and E.R.G.

DECLARATION OF INTERESTS

The authors declare no competing interests.

DECLARATION OF GENERATIVE AI AND AI-ASSISTED TECHNOLOGIES IN THE WRITING PROCESS

During the preparation of this work, the authors used Grammarly to improve grammar. After using this tool/service, the authors reviewed and edited the content as needed and are fully responsible for the publication's content.

STAR★METHODS

Detailed methods are provided in the online version of this paper and include the following:

- KEY RESOURCES TABLE
- EXPERIMENTAL MODEL AND STUDY PARTICIPANT DETAILS
  - Animal studies
  - Cell culture
- METHOD DETAILS
  - cDNA and shRNA
  - Immunofluorescence
  - Immunoblotting
  - Synaptosome fractionation
  - Calcium imaging
  - FM4.64FX dye
  - pHluorin assay
  - GABA and glutamate release
  - Image acquisition
- QUANTIFICATION AND STATISTICAL ANALYSIS
  - Quantitative bioimaging
  - Statistics

SUPPLEMENTAL INFORMATION

Supplemental information can be found online at https://doi.org/10.1016/j.celrep.2025.116005.

Received: July 24, 2024
Revised: April 6, 2025
Accepted: June 23, 2025

REFERENCES

1. Tampellini, D., and Gouras, G.K. (2010). Synapses, synaptic activity and intraneuronal abeta in Alzheimer's disease. Front. Aging Neurosci. *2*, 13. https://doi.org/10.3389/fnagi.2010.00013.

2. Peng, L., Bestard-Lorigados, I., and Song, W. (2022). The synapse as a treatment avenue for Alzheimer's Disease. Mol. Psychiatry *27*, 2940–2949. https://doi.org/10.1038/s41380-022-01565-z.

3. Selkoe, D.J. (2002). Alzheimer's disease is a synaptic failure. Science *298*, 789–791. https://doi.org/10.1126/science.1074069.

4. Meftah, S., and Gan, J. (2023). Alzheimer's disease as a synaptopathy: Evidence for dysfunction of synapses during disease progression. Front. Synaptic Neurosci. *15*, 1129036. https://doi.org/10.3389/fnsyn.2023.1129036.

5. Paula-Lima, A.C., Brito-Moreira, J., and Ferreira, S.T. (2013). Deregulation of excitatory neurotransmission underlying synapse failure in Alzheimer's disease. J. Neurochem. *126*, 191–202. https://doi.org/10.1111/jnc.12304.

6. Palop, J.J., and Mucke, L. (2010). Amyloid-beta-induced neuronal dysfunction in Alzheimer's disease: from synapses toward neural networks. Nat. Neurosci. *13*, 812–818. https://doi.org/10.1038/nn.2583.

7. Noebels, J. (2011). A perfect storm: Converging paths of epilepsy and Alzheimer's dementia intersect in the hippocampal formation. Epilepsia *52*, 39–46. https://doi.org/10.1111/j.1528-1167.2010.02909.x.

8. Goutagny, R., and Krantic, S. (2013). Hippocampal oscillatory activity in Alzheimer's disease: toward the identification of early biomarkers? Aging Dis. *4*, 134–140.

9. Lauterborn, J.C., Scaduto, P., Cox, C.D., Schulmann, A., Lynch, G., Gall, C.M., Keene, C.D., and Limon, A. (2021). Increased excitatory to inhibitory synaptic ratio in parietal cortex samples from individuals with Alzheimer's disease. Nat. Commun. *12*, 2603. https://doi.org/10.1038/s41467-021-22742-8.

10. Targa Dias Anastacio, H., Matosin, N., and Ooi, L. (2022). Neuronal hyperexcitability in Alzheimer's disease: what are the drivers behind this aberrant phenotype? Transl. Psychiatry *12*, 257. https://doi.org/10.1038/s41398-022-02024-7.

11. Perdigão, C., Barata, M.A., Araújo, M.N., Mirfakhar, F.S., Castanheira, J., and Guimas Almeida, C. (2020). Intracellular trafficking mechanisms of synaptic dysfunction in alzheimer's disease. Front. Cell. Neurosci. *14*, 72. https://doi.org/10.3389/fncel.2020.00072.

12. Almeida, C.G., Tampellini, D., Takahashi, R.H., Greengard, P., Lin, M.T., Snyder, E.M., and Gouras, G.K. (2005). Beta-amyloid accumulation in APP mutant neurons reduces PSD-95 and GluR1 in synapses. Neurobiol. Dis. *20*, 187–198. https://doi.org/10.1016/j.nbd.2005.02.008.

13. Snyder, E.M., Nong, Y., Almeida, C.G., Paul, S., Moran, T., Choi, E.Y., Nairn, A.C., Salter, M.W., Lombroso, P.J., Gouras, G.K., and Greengard, P. (2005). Regulation of NMDA receptor trafficking by amyloid-beta. Nat. Neurosci. *8*, 1051–1058. https://doi.org/10.1038/nn1503.

14. Ting, J.T., Kelley, B.G., Lambert, T.J., Cook, D.G., and Sullivan, J.M. (2007). Amyloid precursor protein overexpression depresses excitatory transmission through both presynaptic and postsynaptic mechanisms. Proc. Natl. Acad. Sci. USA *104*, 353–358. https://doi.org/10.1073/pnas.0608807104.

15. Takahashi, R.H., Almeida, C.G., Kearney, P.F., Yu, F., Lin, M.T., Milner, T.A., and Gouras, G.K. (2004). Oligomerization of Alzheimer's β-Amyloid within Processes and Synapses of Cultured Neurons and Brain. J. Neurosci. *24*, 3592–3599. https://doi.org/10.1523/JNEUROSCI.5167-03.2004.

16. Wang, Z., Jackson, R.J., Hong, W., Taylor, W.M., Corbett, G.T., Moreno, A., Liu, W., Li, S., Frosch, M.P., Slutsky, I., et al. (2017). Human Brain-Derived Aβ Oligomers Bind to Synapses and Disrupt Synaptic Activity in a Manner That Requires APP. J. Neurosci. *37*, 11947–11966. https://doi.org/10.1523/JNEUROSCI.2009-17.2017.

17. He, Y., Wei, M., Wu, Y., Qin, H., Li, W., Ma, X., Cheng, J., Ren, J., Shen, Y., Chen, Z., et al. (2019). Amyloid β oligomers suppress excitatory transmitter release via presynaptic depletion of phosphatidylinositol-4,5-bisphosphate. Nat. Commun. *10*, 1193. https://doi.org/10.1038/s41467-019-09114-z.

18. Fogel, H., Frere, S., Segev, O., Bharill, S., Shapira, I., Gazit, N., O'Malley, T., Slomowitz, E., Berdichevsky, Y., Walsh, D.M., et al. (2014). APP homodimers transduce an amyloid-β-mediated increase in release probability at excitatory synapses. Cell Rep. *7*, 1560–1576. https://doi.org/10.1016/j.celrep.2014.04.024.

19. Kurucu, H., Colom-Cadena, M., Davies, C., Wilkins, L., King, D., Rose, J., Tzioras, M., Tulloch, J.H., Smith, C., and Spires-Jones, T.L. (2022). Inhibitory synapse loss and accumulation of amyloid beta in inhibitory presynaptic terminals in Alzheimer's disease. Eur. J. Neurol. *29*, 1311–1323. https://doi.org/10.1111/ene.15043.

20. Willén, K., Sroka, A., Takahashi, R.H., and Gouras, G.K. (2017). Heterogeneous Association of Alzheimer's Disease-Linked Amyloid-β and Amyloid-β Protein Precursor with Synapses. J. Alzheimers Dis. *60*, 511–524. https://doi.org/10.3233/JAD-170262.

21. Milosevic, I. (2018). Revisiting the Role of Clathrin-Mediated Endoytosis in Synaptic Vesicle Recycling. Front. Cell. Neurosci. *12*, 27. https://doi.org/10.3389/fncel.2018.00027.

22. Small, S.A., Simoes-Spassov, S., Mayeux, R., and Petsko, G.A. (2017). Endosomal traffic jams represent a pathogenic hub and therapeutic target in alzheimer's disease. Trends Neurosci. *40*, 592–602. https://doi.org/10.1016/j.tins.2017.08.003.

23. Lambert, J.C., Ibrahim-Verbaas, C.A., Harold, D., Naj, A.C., Sims, R., Bellenguez, C., DeStafano, A.L., Bis, J.C., Beecham, G.W., Grenier-Boley, B., et al. (2013). Meta-analysis of 74,046 individuals identifies 11 new susceptibility loci for Alzheimer's disease. Nat. Genet. *45*, 1452–1458. https://doi.org/10.1038/ng.2802.

24. Seshadri, S., Fitzpatrick, A.L., Ikram, M.A., DeStefano, A.L., Gudnason, V., Boada, M., Bis, J.C., Smith, A.V., Carassquillo, M.M., Lambert, J.C., et al. (2010). Genome-wide analysis of genetic loci associated with Alzheimer disease. JAMA *303*, 1832–1840. https://doi.org/10.1001/jama.2010.574.

25. Taga, M., Petyuk, V.A., White, C., Marsh, G., Ma, Y., Klein, H.-U., Connor, S.M., Kroshilina, A., Yung, C.J., Khairallah, A., et al. (2020). BIN1 protein isoforms are differentially expressed in astrocytes, neurons, and microglia: neuronal and astrocyte BIN1 are implicated in tau pathology. Mol. Neurodegener. *15*, 44. https://doi.org/10.1186/s13024-020-00387-3.

26. Ubelmann, F., Burrinha, T., Salavessa, L., Gomes, R., Ferreira, C., Moreno, N., and Guimas Almeida, C. (2017). Bin1 and CD2AP polarise the endocytic generation of beta-amyloid. EMBO Rep. *18*, 102–122. https://doi.org/10.15252/embr.201642738.

27. Perdigão, C., Barata, M.A., Burrinha, T., and Guimas Almeida, C. (2021). Alzheimer's disease BIN1 coding variants increase intracellular Aβ levels by interfering with BACE1 recycling. J. Biol. Chem. *297*, 101056. https://doi.org/10.1016/j.jbc.2021.101056.

28. Miyagawa, T., Ebinuma, I., Morohashi, Y., Hori, Y., Young Chang, M., Hattori, H., Maehara, T., Yokoshima, S., Fukuyama, T., Tsuji, S., et al. (2016). BIN1 regulates BACE1 intracellular trafficking and amyloid-β production. Hum. Mol. Genet. *25*, 2948–2958. https://doi.org/10.1093/hmg/ddw146.

29. Tan, M.-S., Yu, J.-T., Jiang, T., Zhu, X.-C., Guan, H.-S., and Tan, L. (2014). Genetic variation in BIN1 gene and Alzheimer's disease risk in Han Chinese individuals. Neurobiol. Aging *35*, 1781.e1–1781.e17818. https://doi.org/10.1016/j.neurobiolaging.2014.01.151.

30. Vardarajan, B.N., Ghani, M., Kahn, A., Sheikh, S., Sato, C., Barral, S., Lee, J.H., Cheng, R., Reitz, C., Lantigua, R., et al. (2015). Rare coding mutations identified by sequencing of Alzheimer disease genome-wide association studies loci. Ann. Neurol. *78*, 487–498. https://doi.org/10.1002/ana.24466.

31. Andrew, R.J., De Rossi, P., Nguyen, P., Kowalski, H.R., Recupero, A.J., Guerbette, T., Krause, S.V., Rice, R.C., Laury-Kleintop, L., Wagner, S.L., and Thinakaran, G. (2019). Reduction of the expression of the late-onset Alzheimer's disease (AD) risk-factor BIN1 does not affect amyloid

pathology in an AD mouse model. J. Biol. Chem. *294*, 4477–4487. https://doi.org/10.1074/jbc.RA118.006379.

32. De Rossi, P., Nomura, T., Andrew, R.J., Masse, N.Y., Sampathkumar, V., Musial, T.F., Sudwarts, A., Recupero, A.J., Le Metayer, T., Hansen, M.T., et al. (2020). Neuronal BIN1 regulates presynaptic neurotransmitter release and memory consolidation. Cell Rep. *30*, 3520–3535.e7. https://doi.org/10.1016/j.celrep.2020.02.026.
33. Saha, O., Melo de Farias, A.R., Pelletier, A., Siedlecki-Wullich, D., Landeira, B.S., Gadaut, J., Carrier, A., Vreulx, A.-C., Guyot, K., Shen, Y., et al. (2024). The Alzheimer's disease risk gene BIN1 regulates activity-dependent gene expression in human-induced glutamatergic neurons. Mol. Psychiatry *29*, 2634–2646. https://doi.org/10.1038/s41380-024-02502-y.
34. Schürmann, B., Bermingham, D.P., Kopeikina, K.J., Myczek, K., Yoon, S., Horan, K.E., Kelly, C.J., Martin-de-Saavedra, M.D., Forrest, M.P., Fawcett-Patel, J.M., et al. (2020). A novel role for the late-onset Alzheimer's disease (LOAD)-associated protein Bin1 in regulating postsynaptic trafficking and glutamatergic signaling. Mol. Psychiatry *25*, 2000–2016. https://doi.org/10.1038/s41380-019-0407-3.
35. Voskobiynyk, Y., Roth, J.R., Cochran, J.N., Rush, T., Carullo, N.V., Mesina, J.S., Waqas, M., Vollmer, R.M., Day, J.J., McMahon, L.L., and Roberson, E.D. (2020). Alzheimer's disease risk gene BIN1 induces Tau-dependent network hyperexcitability. eLife *9*, e57354. https://doi.org/10.7554/eLife.57354.
36. Di Paolo, G., Sankaranarayanan, S., Wenk, M.R., Daniell, L., Perucco, E., Caldarone, B.J., Flavell, R., Picciotto, M.R., Ryan, T.A., Cremona, O., and De Camilli, P. (2002). Decreased synaptic vesicle recycling efficiency and cognitive deficits in amphiphysin 1 knockout mice. Neuron *33*, 789–804. https://doi.org/10.1016/s0896-6273(02)00601-3.
37. Butler, M.H., David, C., Ochoa, G.C., Freyberg, Z., Daniell, L., Grabs, D., Cremona, O., and De Camilli, P. (1997). Amphiphysin II (SH3P9; BIN1), a member of the amphiphysin/Rvs family, is concentrated in the cortical cytomatrix of axon initial segments and nodes of ranvier in brain and around T tubules in skeletal muscle. J. Cell Biol. *137*, 1355–1367. https://doi.org/10.1083/jcb.137.6.1355.
38. Glennon, E.B., Lau, D.H.-W., Gabriele, R.M.C., Taylor, M.F., Troakes, C., Opie-Martin, S., Elliott, C., Killick, R., Hanger, D.P., Perez-Nievas, B.G., and Noble, W. (2020). Bridging Integrator-1 protein loss in Alzheimer's disease promotes synaptic tau accumulation and disrupts tau release. Brain Commun. *2*, fcaa011. https://doi.org/10.1093/braincomms/fcaa011.
39. Kato-Negishi, M., Muramoto, K., Kawahara, M., Kuroda, Y., and Ichikawa, M. (2004). Developmental changes of GABAergic synapses formed between primary cultured cortical neurons. Brain Res. Dev. Brain Res. *152*, 99–108. https://doi.org/10.1016/j.devbrainres.2004.05.013.
40. Murphy, T.H., Blatter, L.A., Wier, W.G., and Baraban, J.M. (1992). Spontaneous synchronous synaptic calcium transients in cultured cortical neurons. J. Neurosci. *12*, 4834–4845. https://doi.org/10.1523/JNEUROSCI.12-12-04834.1992.
41. Serra, M., Guaraldi, M., and Shea, T.B. (2010). Inhibitory neurons modulate spontaneous signaling in cultured cortical neurons: density-dependent regulation of excitatory neuronal signaling. Phys. Biol. *7*, 026009. https://doi.org/10.1088/1478-3975/7/2/026009.
42. Das, P., Bell-Horner, C.L., Machu, T.K., and Dillon, G.H. (2003). The GABA (A) receptor antagonist picrotoxin inhibits 5-hydroxytryptamine type 3A receptors. Neuropharmacology *44*, 431–438. https://doi.org/10.1016/s0028-3908(03)00032-7.
43. Turrigiano, G. (2011). Too many cooks? Intrinsic and synaptic homeostatic mechanisms in cortical circuit refinement. Annu. Rev. Neurosci. *34*, 89–103. https://doi.org/10.1146/annurev-neuro-060909-153238.
44. Helassa, N., Dürst, C.D., Coates, C., Kerruth, S., Arif, U., Schulze, C., Wiegert, J.S., Geeves, M., Oertner, T.G., and Török, K. (2018). Ultrafast glutamate sensors resolve high-frequency release at Schaffer collateral synapses. Proc. Natl. Acad. Sci. USA *115*, 5594–5599. https://doi.org/10.1073/pnas.1720648115.
45. Yao, J., Nowack, A., Kensel-Hammes, P., Gardner, R.G., and Bajjalieh, S.M. (2010). Cotrafficking of SV2 and synaptotagmin at the synapse. J. Neurosci. *30*, 5569–5578. https://doi.org/10.1523/JNEUROSCI.4781-09.2010.
46. Sarkis, R.A. (2022). Levetiracetam in alzheimer's disease: do epileptologists already have the cure? Epilepsy Curr. *22*, 225–227. https://doi.org/10.1177/15357597221096020.
47. Sen, A., Akinola, M., Tai, X.Y., Symmonds, M., Davis Jones, G., Mura, S., Galloway, J., Hallam, A., Chan, J.Y.C., Koychev, I., et al. (2021). An Investigation of Levetiracetam in Alzheimer's Disease (ILiAD): a double-blind, placebo-controlled, randomised crossover proof of concept study. Trials *22*, 508. https://doi.org/10.1186/s13063-021-05404-4.
48. Vossel, K., Ranasinghe, K.G., Beagle, A.J., La, A., Ah Pook, K., Castro, M., Mizuiri, D., Honma, S.M., Venkateswaran, N., Koestler, M., et al. (2021). Effect of levetiracetam on cognition in patients with alzheimer disease with and without epileptiform activity: A randomized clinical trial. JAMA Neurol. *78*, 1345–1354. https://doi.org/10.1001/jamaneurol.2021.3310.
49. Xiao, R. (2016). Levetiracetam might act as an efficacious drug to attenuate cognitive deficits of Alzheimer's disease. Curr. Top. Med. Chem. *16*, 565–573. https://doi.org/10.2174/1568026615666150813144603.
50. Chanaday, N.L., Cousin, M.A., Milosevic, I., Watanabe, S., and Morgan, J.R. (2019). The Synaptic Vesicle Cycle Revisited: New Insights into the Modes and Mechanisms. J. Neurosci. *39*, 8209–8216. https://doi.org/10.1523/JNEUROSCI.1158-19.2019.
51. Rizzoli, S.O. (2014). Synaptic vesicle recycling: steps and principles. EMBO J. *33*, 788–822. https://doi.org/10.1002/embj.201386357.
52. Saheki, Y., and De Camilli, P. (2012). Synaptic vesicle endocytosis. Cold Spring Harb. Perspect. Biol. *4*, a005645. https://doi.org/10.1101/cshperspect.a005645.
53. Wu, Y., O'Toole, E.T., Girard, M., Ritter, B., Messa, M., Liu, X., McPherson, P.S., Ferguson, S.M., and De Camilli, P. (2014). A dynamin 1-dynamin 3- and clathrin-independent pathway of synaptic vesicle recycling mediated by bulk endocytosis. eLife *3*, e01621. https://doi.org/10.7554/eLife.01621.
54. de Hoop, M.J., Huber, L.A., Stenmark, H., Williamson, E., Zerial, M., Parton, R.G., and Dotti, C.G. (1994). The involvement of the small GTP-binding protein Rab5a in neuronal endocytosis. Neuron *13*, 11–22. https://doi.org/10.1016/0896-6273(94)90456-1.
55. Megías, M., Emri, Z., Freund, T.F., and Gulyás, A.I. (2001). Total number and distribution of inhibitory and excitatory synapses on hippocampal CA1 pyramidal cells. Neuroscience *102*, 527–540. https://doi.org/10.1016/s0306-4522(00)00496-6.
56. Bae, J.R., Lee, W., Jo, Y.O., Han, S., Koh, S., Song, W.K., and Kim, S.H. (2020). Distinct synaptic vesicle recycling in inhibitory nerve terminals is coordinated by SV2A. Prog. Neurobiol. *194*, 101879. https://doi.org/10.1016/j.pneurobio.2020.101879.
57. Marvin, J.S., Shimoda, Y., Magloire, V., Leite, M., Kawashima, T., Jensen, T.P., Kolb, I., Knott, E.L., Novak, O., Podgorski, K., et al. (2019). A genetically encoded fluorescent sensor for in vivo imaging of GABA. Nat. Methods *16*, 763–770. https://doi.org/10.1038/s41592-019-0471-2.
58. van Oostrum, M., Blok, T.M., Giandomenico, S.L., Tom Dieck, S., Tushev, G., Fürst, N., Langer, J.D., and Schuman, E.M. (2023). The proteomic landscape of synaptic diversity across brain regions and cell types. Cell *186*, 5411–5427.e23. https://doi.org/10.1016/j.cell.2023.09.028.
59. Karlsson, M., Zhang, C., Méar, L., Zhong, W., Digre, A., Katona, B., Sjöstedt, E., Butler, L., Odeberg, J., Dusart, P., et al. (2021). A single-cell type transcriptomics map of human tissues. Sci. Adv. *7*, eabh2169. https://doi.org/10.1126/sciadv.abh2169.

60. Grønborg, M., Pavlos, N.J., Brunk, I., Chua, J.J.E., Münster-Wandowski, A., Riedel, D., Ahnert-Hilger, G., Urlaub, H., and Jahn, R. (2010). Quantitative comparison of glutamatergic and GABAergic synaptic vesicles unveils selectivity for few proteins including MAL2, a novel synaptic vesicle protein. J. Neurosci. *30*, 2–12. https://doi.org/10.1523/JNEUROSCI.4074-09.2010.

61. Garcia, J.D., Gookin, S.E., Crosby, K.C., Schwartz, S.L., Tiemeier, E., Kennedy, M.J., Dell'Acqua, M.L., Herson, P.S., Quillinan, N., and Smith, K.R. (2021). Stepwise disassembly of GABAergic synapses during pathogenic excitotoxicity. Cell Rep. *37*, 110142. https://doi.org/10.1016/j.celrep.2021.110142.

62. Benfenati, F., Valtorta, F., Rubenstein, J.L., Gorelick, F.S., Greengard, P., and Czernik, A.J. (1992). Synaptic vesicle-associated Ca2+/calmodulin-dependent protein kinase II is a binding protein for synapsin I. Nature *359*, 417–420. https://doi.org/10.1038/359417a0.

63. Baldelli, P., Fassio, A., Valtorta, F., and Benfenati, F. (2007). Lack of synapsin I reduces the readily releasable pool of synaptic vesicles at central inhibitory synapses. J. Neurosci. *27*, 13520–13531. https://doi.org/10.1523/JNEUROSCI.3151-07.2007.

64. Terada, S., Tsujimoto, T., Takei, Y., Takahashi, T., and Hirokawa, N. (1999). Impairment of inhibitory synaptic transmission in mice lacking synapsin I. J. Cell Biol. *145*, 1039–1048. https://doi.org/10.1083/jcb.145.5.1039.

65. Santos, M.S., Park, C.K., Foss, S.M., Li, H., and Voglmaier, S.M. (2013). Sorting of the vesicular GABA transporter to functional vesicle pools by an atypical dileucine-like motif. J. Neurosci. *33*, 10634–10646. https://doi.org/10.1523/JNEUROSCI.0329-13.2013.

66. Calafate, S., Flavin, W., Verstreken, P., and Moechars, D. (2016). Loss of bin1 promotes the propagation of tau pathology. Cell Rep. *17*, 931–940. https://doi.org/10.1016/j.celrep.2016.09.063.

67. Kajiho, H., Saito, K., Tsujita, K., Kontani, K., Araki, Y., Kurosu, H., and Katada, T. (2003). RIN3: a novel Rab5 GEF interacting with amphiphysin II involved in the early endocytic pathway. J. Cell Sci. *116*, 4159–4168. https://doi.org/10.1242/jcs.00718.

68. Shimizu, H., Kawamura, S., and Ozaki, K. (2003). An essential role of Rab5 in uniformity of synaptic vesicle size. J. Cell Sci. *116*, 3583–3590. https://doi.org/10.1242/jcs.00676.

69. Voglmaier, S.M., Kam, K., Yang, H., Fortin, D.L., Hua, Z., Nicoll, R.A., and Edwards, R.H. (2006). Distinct endocytic pathways control the rate and extent of synaptic vesicle protein recycling. Neuron *51*, 71–84. https://doi.org/10.1016/j.neuron.2006.05.027.

70. Xu, Y., Zhao, M., Han, Y., and Zhang, H. (2020). Gabaergic inhibitory interneuron deficits in alzheimer's disease: implications for treatment. Front. Neurosci. *14*, 660. https://doi.org/10.3389/fnins.2020.00660.

71. Burrinha, T., Martinsson, I., Gomes, R., Terrasso, A.P., Gouras, G.K., and Almeida, C.G. (2021). Upregulation of APP endocytosis by neuronal aging drives amyloid-dependent synapse loss. J. Cell Sci. *134*, jcs255752. https://doi.org/10.1242/jcs.255752.

72. Mirfakhar, F.S., Castanheira, J., Domingues, R., Ramalho, J.S., and Guimas Almeida, C. (2024). The Alzheimer's Disease Risk Gene CD2AP Functions in Dendritic Spines by Remodeling F-Actin. J. Neurosci. *44*, e1734232024. https://doi.org/10.1523/JNEUROSCI.1734-23.2024.

73. Garcia-Agudo, L.F., Shi, Z., Smith, I.F., Kramár, E.A., Tran, K., Kawauchi, S., Wang, S., Collins, S., Walker, A., Shi, K.-X., et al. (2024). BIN1K358R suppresses glial response to plaques in mouse model of Alzheimer's disease. Alzheimer's Dement. *20*, 2922–2942. https://doi.org/10.1002/alz.13767.

74. Malki, I., Cantrelle, F.-X., Sottejeau, Y., Lippens, G., Lambert, J.-C., and Landrieu, I. (2017). Regulation of the interaction between the neuronal BIN1 isoform 1 and Tau proteins - role of the SH3 domain. FEBS J. *284*, 3218–3229. https://doi.org/10.1111/febs.14185.

75. Kojima, C., Hashimoto, A., Yabuta, I., Hirose, M., Hashimoto, S., Kanaho, Y., Sumimoto, H., Ikegami, T., and Sabe, H. (2004). Regulation of Bin1 SH3 domain binding by phosphoinositides. EMBO J. *23*, 4413–4422. https://doi.org/10.1038/sj.emboj.7600442.

76. Leprince, C., Romero, F., Cussac, D., Vayssiere, B., Berger, R., Tavitian, A., and Camonis, J.H. (1997). A new member of the amphiphysin family connecting endocytosis and signal transduction pathways. J. Biol. Chem. *272*, 15101–15105. https://doi.org/10.1074/jbc.272.24.15101.

77. Ramjaun, A.R., Micheva, K.D., Bouchelet, I., and McPherson, P.S. (1997). Identification and characterization of a nerve terminal-enriched amphiphysin isoform. J. Biol. Chem. *272*, 16700–16706. https://doi.org/10.1074/jbc.272.26.16700.

78. Celone, K.A., Calhoun, V.D., Dickerson, B.C., Atri, A., Chua, E.F., Miller, S.L., DePeau, K., Rentz, D.M., Selkoe, D.J., Blacker, D., et al. (2006). Alterations in memory networks in mild cognitive impairment and Alzheimer's disease: an independent component analysis. J. Neurosci. *26*, 10222–10231. https://doi.org/10.1523/JNEUROSCI.2250-06.2006.

79. Dickerson, B.C., Salat, D.H., Bates, J.F., Atiya, M., Killiany, R.J., Greve, D.N., Dale, A.M., Stern, C.E., Blacker, D., Albert, M.S., and Sperling, R.A. (2004). Medial temporal lobe function and structure in mild cognitive impairment. Ann. Neurol. *56*, 27–35. https://doi.org/10.1002/ana.20163.

80. Hämäläinen, A., Pihlajamäki, M., Tanila, H., Hänninen, T., Niskanen, E., Tervo, S., Karjalainen, P.A., Vanninen, R.L., and Soininen, H. (2007). Increased fMRI responses during encoding in mild cognitive impairment. Neurobiol. Aging *28*, 1889–1903. https://doi.org/10.1016/j.neurobiolaging.2006.08.008.

81. Putcha, D., Brickhouse, M., O'Keefe, K., Sullivan, C., Rentz, D., Marshall, G., Dickerson, B., and Sperling, R. (2011). Hippocampal hyperactivation associated with cortical thinning in Alzheimer's disease signature regions in non-demented elderly adults. J. Neurosci. *31*, 17680–17688. https://doi.org/10.1523/JNEUROSCI.4740-11.2011.

82. Palop, J.J., and Mucke, L. (2009). Epilepsy and cognitive impairments in Alzheimer disease. Arch. Neurol. *66*, 435–440. https://doi.org/10.1001/archneurol.2009.15.

83. Balint, B., and Bhatia, K.P. (2016). Stiff person syndrome and other immune-mediated movement disorders - new insights. Curr. Opin. Neurol. *29*, 496–506. https://doi.org/10.1097/WCO.0000000000000351.

84. Bakker, A., Krauss, G.L., Albert, M.S., Speck, C.L., Jones, L.R., Stark, C.E., Yassa, M.A., Bassett, S.S., Shelton, A.L., and Gallagher, M. (2012). Reduction of hippocampal hyperactivity improves cognition in amnestic mild cognitive impairment. Neuron *74*, 467–474. https://doi.org/10.1016/j.neuron.2012.03.023.

85. Schindelin, J., Arganda-Carreras, I., Frise, E., Kaynig, V., Longair, M., Pietzsch, T., Preibisch, S., Rueden, C., Saalfeld, S., Schmid, B., et al. (2012). Fiji: an open-source platform for biological-image analysis. Nat. Methods *9*, 676–682. https://doi.org/10.1038/nmeth.2019.

86. de Chaumont, F., Dallongeville, S., Chenouard, N., Hervé, N., Pop, S., Provoost, T., Meas-Yedid, V., Pankajakshan, P., Lecomte, T., Le Montagner, Y., et al. (2012). Icy: an open bioimage informatics platform for extended reproducible research. Nat. Methods *9*, 690–696. https://doi.org/10.1038/nmeth.2075.

87. Stirling, D.R., Carpenter, A.E., and Cimini, B.A. (2021). CellProfiler Analyst 3.0: accessible data exploration and machine learning for image analysis. Bioinformatics *37*, 3992–3994. https://doi.org/10.1093/bioinformatics/btab634.

88. Bardy, C., van den Hurk, M., Eames, T., Marchand, C., Hernandez, R.V., Kellogg, M., Gorris, M., Galet, B., Palomares, V., Brown, J., et al. (2015). Neuronal medium that supports basic synaptic functions and activity of human neurons in vitro. Proc. Natl. Acad. Sci. USA *112*, E2725–E2734. https://doi.org/10.1073/pnas.1504393112.

89. Nowack, A., Malarkey, E.B., Yao, J., Bleckert, A., Hill, J., and Bajjalieh, S.M. (2011). Levetiracetam reverses synaptic deficits produced by overexpression of SV2A. PLoS One *6*, e29560. https://doi.org/10.1371/journal.pone.0029560.

90. Sartori, M., Mendes, T., Desai, S., Lasorsa, A., Herledan, A., Malmanche, N., Mäkinen, P., Marttinen, M., Malki, I., Chapuis, J., et al. (2019). BIN1 recovers tauopathy-induced long-term memory deficits in mice and interacts with Tau through Thr348 phosphorylation. Acta Neuropathol. *138*, 631–652. https://doi.org/10.1007/s00401-019-02017-9.

91. Burrinha, T., Cunha, C., Hall, M.J., Lopes-da-Silva, M., Seabra, M.C., and Guimas Almeida, C. (2023). Deacidification of endolysosomes by neuronal aging drives synapse loss. Traffic *24*, 334–354. https://doi.org/10.1111/tra.12889.

92. Ryan, T.A., Reuter, H., Wendland, B., Schweizer, F.E., Tsien, R.W., and Smith, S.J. (1993). The kinetics of synaptic vesicle recycling measured at single presynaptic boutons. Neuron *11*, 713–724. https://doi.org/10.1016/0896-6273(93)90081-2.

93. Burrone, J., Li, Z., and Murthy, V.N. (2006). Studying vesicle cycling in presynaptic terminals using the genetically encoded probe synaptopHluorin. Nat. Protoc. *1*, 2970–2978. https://doi.org/10.1038/nprot.2006.449.

94. Sambri, I., D'Alessio, R., Ezhova, Y., Giuliano, T., Sorrentino, N.C., Cacace, V., De Risi, M., Cataldi, M., Annunziato, L., De Leonibus, E., and Fraldi, A. (2017). Lysosomal dysfunction disrupts presynaptic maintenance and restoration of presynaptic function prevents neurodegeneration in lysosomal storage diseases. EMBO Mol. Med. *9*, 112–132. https://doi.org/10.15252/emmm.201606965.

95. Arshadi, C., Günther, U., Eddison, M., Harrington, K.I.S., and Ferreira, T.A. (2021). SNT: a unifying toolbox for quantification of neuronal anatomy. Nat. Methods *18*, 374–377. https://doi.org/10.1038/s41592-021-01105-7.

96. Arganda-Carreras, I., Fernández-González, R., Muñoz-Barrutia, A., and Ortiz-De-Solorzano, C. (2010). 3D reconstruction of histological sections: Application to mammary gland tissue. Microsc. Res. Tech. *73*, 1019–1029. https://doi.org/10.1002/jemt.20829.

STAR★METHODS

KEY RESOURCES TABLE

REAGENT or RESOURCE	SOURCE	IDENTIFIER
Antibodies		
Mouse monoclonal anti-Bin1 1:100 (IF), 1:1000 (WB), 1:80 (IHC)	Millipore	Cat#05-449; RRID:AB_309738
Rabbit monoclonal anti-Bin1 1:100 (IF)	Abcam	Cat#ab182562; RRID:AB_3669062
Rabbit polyclonal anti-synapsin I 1:250 (IF), 1:1000 (WB)	Abcam	Cat#ab8; RRID:AB_2200097
Rabbit polyclonal anti-PSD-95 1:200 (IF), 1:1000 (WB)	Millipore	Cat#AB9708; RRID:AB_2092543
Guinea Pig polyclonal anti-vGLUT1 1:200 (IF), 1:500 (IHC)	SynapticSystems	Cat#135 304; RRID:AB_887878
Rabbit polyclonal anti-vGAT 1:500 (IF), 1:200 (IHC)]	Merck Millipore	Cat#AB5062P; RRID:AB_2301998
Mouse monoclonal anti-gephyrin 1:250 (IF)	SynapticSystems	Cat#147 011; RRID:AB_2810215
Mouse monoclonal anti-tubulin 1:10,000 (WB)	Millipore	Cat#MAB1637; RRID:AB_2210524
Goat monoclonal anti-GAPDH 1:10000 (WB)	Sicgen	Cat#ab0049; RRID:AB_2333142
Mouse monoclonal anti-c-Myc 1:500 (IF)	Thermo Fisher Scientific	Cat#13-2500; RRID:AB_2533008
Goat polyclonal anti-Rab5 1:200 (IF)	Sicgen	Cat#ab1024; RRID: AB_2333166
Rabbit polyclonal anti-SV2A 1:200 (IF)	SynapticSystems	Cat#119 002; RRID:AB_887802
Chemicals, peptides, and recombinant proteins		
Heat-Inactivated FBS	Thermo Fisher Scientific	Cat#16140-071
poly-D-lysine	Sigma-Aldrich	Cat#P1149
Brainphys Neuronal Medium-SM1	STEMCELL Technologies	Cat#05792
Neurobasal medium	Thermo Fisher Scientific	Cat#21103049
B-27	Thermo Fisher Scientific	Cat#17504044
Glutamax	Thermo Fisher Scientific	Cat#35050-038
penicillin-streptomycin	Thermo Fisher Scientific	Cat#15140-122
Lipofectamine2000	Thermo Fisher Scientific	Cat#11668019
Fetal Bovine Serum	Sigma- Aldrich	Cat#F0804
DAPT	Calbiochem	Cat#565770
β-Secretase Inhibitor IV	Calbiochem	Cat#565788
DMSO	PanReac AppliChem	Cat#A3672.0100
Levetiracetam	Sigma-Aldrich	Cat#L8668
Lenti-X concentrator	Takara	Cat#631231
Fura-Red	Thermo Fisher Scientific	Cat#F3021
6-cyano-7-nitroquinoxaline-2,3-dione	Sigma-Aldrich	Cat#C127
D, L-2-amino-5-phosphonovaleric acid	Sigma-Aldrich	Cat#A5282
FM4-64FX	Thermo Fisher Scientific	Cat#F34653
Fluoromount-G	Southern Biotechnology	Cat#00-4958-02
DAPI	Sigma	Cat#D9542
Experimental models: Cell lines		
N2a	Z. Lenkei (IPNP)	ATCC®CCL-131™
Experimental models: Organisms/strains		
Mouse/ BALB/c	Charles River	BALB/cByJ
Recombinant DNA		
vGAT-pHluorin	SH Kim (Kyung Hee University)	N/A
vGLUT1-pHluorin	SH Kim	N/A
pCI syn iGluu	Addgene	Cat#106122
pGP-CAG-iGABASnFR2-WPRE-bGH-polyA	Addgene	Cat#218868
nBin1-myc	In house	[27]

(*Continued on next page*)

Continued

REAGENT or RESOURCE	SOURCE	IDENTIFIER
nBin1^{PL}-myc	In house	
nBin1^{KR}-myc	In house	
shBin1^{0}	Sigma	TRCN0000380696
shBin1^{1}	Sigma	TRCN0000380439
shBin1^{2}	Sigma	TRCN0000088191
TurboGFP^{TM} Positive Control Plasmid DNA	Sigma	Cat#SHC003
pGFP-C-shLenti	OriGene Technologies	Cat#NC1766994
psPAX2	D Trono(EPFL)	Cat#12260
pMD2.G	D Trono(EPFL)	Cat#12259
Software and algorithms		
Fiji (version 1.53)	NIH	https://fiji.sc/[85]
Time Series Analyzer-V3	Balaji-J	https://imagej.net/ij/plugins/time-series.html
ICY	Institut Pasteur and France-BioImaging	Icy.bioimageanalysis.org [86]
IMARIS (version 9.5.0)	Oxford Instruments	https://imaris.oxinst.com/
ComDet v.0.5.5	*Katrukha*	https://github.com/ekatrukha/ComDet
GraphPad (version 8.4.0)	Dotmatics	www.graphpad.com
CellProfiler (version 4.2.1)	Cimini lab (Broad Institute)	www.cellprofiler.org[87]

EXPERIMENTAL MODEL AND STUDY PARTICIPANT DETAILS

Animal studies

All animal procedures were performed according to EU recommendations and were approved by the Ethical Committee, the NMS – Universidade Nova de Lisboa ethical committee (162/2021/CEFCM), and the NOVA Medical School Animal Welfare Body (ORBEA).

Cell culture

Primary neuronal cultures from *Mus musculus* were prepared as previously[71,88] from cortices of embryonic day 16 (E16) wild-type BALB/c mice of either sex. Brain tissue was pooled and dissociated briefly by trypsinization and trituration in Dulbecco's medium Eagle medium (DMEM) with 10% fetal bovine serum. Dissociated neurons were plated in DMEM with 10% FBS on poly-D-lysine-coated 6-well plates (3x10^5 cells), 13-inch glass coverslips (5x10^4 cells), 18-inch glass coverslip (2x10^5 cells), u-Slide 8 Well chamber slides (ibidi) (5x10^4 cells). After 16 h, the medium was replaced with Brainphys Neuronal Medium supplemented with SM1, which promotes synaptic activity,[88] or in the initial Bin1 localization experiments, with Neurobasal medium supplemented with B-27, GlutaMAX, and penicillin-streptomycin. Neurons were maintained at 37°C in 5% CO_2 for 15 days *in vitro* (DIV) in complete Brainphys media (21 DIV in Neurobasal). For cDNA expression, primary neurons were transiently transfected on 8 DIV with 1 μg (4 μg for 25–35 mm dishes) of cDNA with Lipofectamine 2000. Primary neurons (8 DIV) were transduced with lentiviral constructs for 5 min at 37°C in 5% CO2 for shRNA treatment. Afterward, the media was half replaced with conditioned, half-fresh, complete Brainphys media. For rescue experiments, neurons were subsequently transiently transfected with cDNA at 11 DIV. For live imaging, neurons cultured on 18-inch coverslips were placed in Tyrode solution in a magnetic chamber (Chamlide CMB; Live Cell Instrument, SK).

Neuroblastoma Neuro2a (N2a) cells were cultured in DMEM-GlutaMAX with 10% FBS at 37°C in 5% CO2, plated in coated 6-well plates (2x10^5 cells). N2a cells were transduced with lentiviral constructs expressing shRNA and analyzed 72 h post-transduction.

When indicated, γ-secretase was inhibited by 24 h treatment with 250 nM DAPT, BACE1 was inhibited by 24 h treatment with 10 μM compound IV (BACEi), and DMSO (0.1%; solvent) was used as a control. When indicated, neurons were incubated for 16 h with 100 μM Levetiracetam.[89]

METHOD DETAILS

cDNA and shRNA

To KD Bin1 expression, Mission pLKO,1-puro-CMV-shRNA vectors targeting BIN1: shBin1^0 (TRCN0000380696: CTTCCATAAAGA GATG); shBin1^1 (TRCN0000380439[90]: CTGATGAGCTGCAACTCAA); and shBin1^2 (TRCN0000088191[66]: CTTCCATAAAGAGATG), were transduced using lentiviral particles. Non-targeting shRNA was used as control (shControl); SHC003 or pGFP-C-shLenti. Vectors were packaged in lentivirus (LVs) by co-transfection with psPAX2 and pMD2.G, along with helper plasmids, in STAR-RDpro cells (ECACC 04072117). LVs were collected by centrifugation and purified with the Lenti-X concentrator according to the manufacturer's

protocol. Each lentiviral batch was titrated to assess the optimum volume for transduction. We relied on the signal of the TurboGFP tag of shRNA to identify KD neurons whenever possible. Otherwise, we assumed that all neurons had some level of Bin1 depletion, as primary neurons consistently exhibited a 50% reduction in Bin1 levels, as determined by Western blot and immunofluorescence. To follow Bin1 levels during neuronal differentiation until 20 DIV in Brainphys, primary neurons were plated at 2×10^5 cells per well.

For the pHluorin assays, primary neurons were transfected at 8 DIV and transduced with shRNA at 11 DIV, as described above.

Immunofluorescence

Immunofluorescence was performed as previously.[26] Cultured primary neurons were fixed with 4% paraformaldehyde and 4% sucrose in PBS for 20 min, permeabilized with 0.3% Triton X-100 in PBS for 15 min, and blocked in 0.1% saponin, 2% FBS, 1% bovine serum albumin (BSA) in PBS for 1 h at room temperature before antibody incubation using standard procedure. To assess Bin1 localization under neuronal activity, neurons at 15 DIV were stimulated with 90 mM KCl.[53] Firstly, the neurons were rinsed with Ca^{2+}-free Tyrode solution [119 mM NaCl, 2.5 mM KCl, 2 mM $MgCl_2$, 25 mM HEPES, 30 mM glucose pH 7.4] prewarmed to 37°C. Tyrode buffer containing 2 mM $CaCl_2$ and 2.5 mM or 90 mM KCl (37°C) was applied to neurons for 90 s before fixation. NaCl concentration was adapted to maintain ionic balance. Fixed sagittal sections, 40 μm thick, were sliced on a microtome (Cryostat Leica CM3050 S) from a gelatin-embedded forebrain of the left hemisphere of 6-month-old (adult) brains. Sections were washed in 0.1 M phosphate buffer (PB), permeabilized with 0.3% Triton X-100 in 0.1 M PB for 10 min, and blocked in 0.3% Triton X-100 and 5% BSA in 0.1 M PB for 1 h at room temperature before primary antibody incubation in blocking solution for 16 h at 4°C. DAPI was added to the secondary antibody solution. Coverslips were mounted using Fluoromount-G.

Immunoblotting

Cell lysates were prepared using modified RIPA buffer [50 mM Tris-HCl (pH 7.4), 150 mM NaCl, 1% NP-40, 0.25% sodium deoxycholate, 1 mM EGTA, 0.1% SDS, and protease inhibitor cocktail (PIC)]. Briefly, cells were washed with ice-cold PBS, scraped in a modified RIPA buffer (100 μL/35 mm) after 5 min, and then placed on ice for 15 min before 5min centrifugation at 13,300 rpm at 4°C. Proteins were mixed with sample buffer, heated to 95°C for 5 min, and then run on a 7.5% Tris-glycine SDS-PAGE gel. The proteins were transferred to nitrocellulose membranes (GE Healthcare). After immunoblotting, detection was done using an ECL Prime kit (GE Healthcare). Images of immunoblots were captured using a ChemiDoc Gel Imaging System (Bio-Rad) within the linear range and quantified by densitometry using the 'Analyze gels' function in Fiji software.

Synaptosome fractionation

Synaptosomes were prepared from frozen forebrains (including cortex and hippocampus) of 6-month-old (adult) female BALB/c mice as previously.[91] Synaptosomes were prepared from primary neurons using 1.8×10^6 cells. All steps were performed at 4°C. Brain tissue was homogenized with a pestle in ice-cold 0.32 M sucrose (Sigma-Aldrich), 10 mM HEPES; and 1× PIC pH 7.4 (10 mL buffer/gram of tissue). Neuronal cells at 15 DIV were washed with ice-cold 1X PBS and gently scraped with 0.32 M sucrose, 10 mM HEPES, 1× PIC, pH 7.4. The homogenate was centrifuged twice for 10 min at 1,000 × g to pellet the nuclear fractions. The supernatant was centrifuged for 15 min at 10,000 × g to generate a crude synaptosome pellet. This pellet was resuspended in 1 mL of 4 mM HEPES, 1 mM EDTA, PIC 1X, pH 7.4, and then re-spun twice at 10,000 × g for 15 min to pellet the washed crude synaptosomal pellet. The pellet was lysed in 1 mL of 20 mM HEPES, 100 mM NaCl, 0.5% Triton X-100, PIC 1X, pH 7.2, and let under head-over-heel rotation at 4°C for 30 min. Furthermore, it was centrifuged for 20 min at 12,000× g to pellet the synaptosomal membrane fraction. The supernatant contains crude SV. All pellets were resuspended in 100 μL of modified RIPA buffer. Equivalent amounts of protein, as determined by the BCA protein assay kit (Thermo Fisher Scientific), were mixed with sample buffer, heated at 95°C for 5 min, and ran on a 7.5% Tris-glycine SDS-PAGE.

Calcium imaging

To follow calcium imaging, neurons were incubated with 5 μM Fura Red in complete Brainphys media for 30 min at 37°C in 5% CO_2 (adapted from[39]). Before imaging, cells were washed three times in a modified Tyrode solution [130 mM NaCl, 5.4 mM KCl, 1 mM $MgCl_2$, 1.8 mM $CaCl_2$, 20 mM HEPES, 5.5 mM glucose pH 7.4]. Neuronal calcium transients were recorded for 3 min, basal activity. 10 μM Picrotoxin (PTX) in Tyrode solution or 100 μM Levetiracetam was added as indicated, and calcium transients were recorded for 3 min.[39] During imaging, the temperature was maintained at 37°C using a temperature-controlled incubator. Images were analyzed using the Time Series Analyzer V3 plugin in Fiji. Briefly, regions of interest (ROIs) were placed on neuronal somas, and integrated density was measured per frame. The baseline was normalized to the average of 100 frames with the lowest intensity (F0). ΔF/F0 [(F-F0)/F0] was calculated and represented in GraphPad Prism software to obtain the area under each calcium peak and measure spike frequency and amplitude. Peaks with more than 25% of the maximum peak were considered. Fura Red mean intensity is the average total intensity obtained in each frame during basal activity after background subtraction.

FM4.64FX dye

Labeling active synapses with FM4.64FX was done as described previously.[72] The styryl dye FM4-64FX at 10 μM in high potassium solution [119 mM NaCl, 70 mM KCl, 2 mM $MgCl_2$, 2 mM $CaCl_2$, 5 mM HEPES, 30 mM glucose pH 7.4] was applied to neurons for 90s,[92] washed for 1 min in Tyrode solution with low Ca^{2+} and containing 1 μM tetrodotoxin (TTX) [150 mM NaCl, 5 mM KCl, 5 mM

$MgCl_2$, 0.2 mM $CaCl_2$, 5 mM HEPES, 30 mM glucose pH 7.4] and in PBS, before fixation with 2% paraformaldehyde and 4% sucrose in PBS for 10min and mounted.

After labeling and washing for 5 min in Tyrode solution, live imaging was performed for 60 s. Images were acquired at 2 s per frame and analyzed using the Fiji plugin 'Time Series Analyzer V3'. Briefly, circular ROIs were positioned over each bouton, and the integrated intensity was measured in each frame of the time series. To assess the unloading of the FM dye, the fluorescence after 2 and 60 s (F_{unload}) was normalized to the last frame of loading (F_{load}).

pHluorin assay

To directly measure synaptic exocytosis and endocytosis, we used the pHluorin assay[93,94] and imaged vGAT/vGLUT1-pHluorin positive neurons. First, neurons were imaged at steady state for 30 s in Tyrode solution [119 mM NaCl, 2.5 mM KCl, 2 mM $MgCl_2$, 2 mM $NaCl_2$, 25 mM HEPES, 30 mM glucose, pH 7.4] with 10 μM 6-cyano-7-nitroquinoxaline-2,3-dione (CQNX) and 50 μM D, L-2-amino-5-phosphonovaleric acid (AP5). Second, after stimulation in a high potassium solution (50 mM), neurons were imaged for 60s. Finally, neurons were imaged upon adding 50 mM NH_4Cl (pH 8) for 50 s. Images were acquired at a rate of one frame every 3 s. The images were analyzed using the Fiji plugin 'Time Series Analyzer V3' after bleach correction (simple Ratio method). The integrated fluorescence of each bouton at the indicated time (F) was expressed as $\Delta F/\Delta F_{NH4Cl}$ [(F-F0)/(F_{NH4Cl}-F0)]. F0 was defined as the average fluorescence of the last five frames before KCl stimulation, and F_{NH4Cl} was defined as the fluorescence of the first frame after adding NH_4Cl. Presynaptic terminals exhibiting a fluorescence increase with KCl stimulation of less than 50% of the average fluorescence of all boutons were excluded from the analysis. The endocytic constant τ (s) was obtained using GraphPad Prism version 8.4.0 in a nonlinear regression analysis, which involved fitting a one-phase decay to the $\Delta F/\Delta F_{NH4Cl}$ curve upon KCl stimulation.

GABA and glutamate release

To measure GABA or glutamate release, we imaged the GABA sensor, iGABASnFR2, or the glutamate sensor, iGluu, in neurons expressing these sensors. Neurons were imaged at steady state for 30 s in Tyrode solution [119 mM NaCl, 2.5 mM KCl, 2 mM $MgCl_2$, 2 mM $CaCl_2$, 25 mM HEPES, 30 mM glucose, pH 7.4]. After stimulation in a high potassium solution (50 mM), the neurons were imaged for 30 s. Images were acquired at a rate of 1 frame every 3 s. The images were analyzed using the plugin 'Time Series Analyzer V3' after bleach correction (simple Ratio method). The integrated fluorescence of each bouton at the indicated time (F) was expressed as ΔF, F-F0, where F represents the fluorescence at a given time, and F0 is the average fluorescence of the frames before KCl stimulation.

Image acquisition

Epifluorescence microscopy was performed on a wide-field upright microscope, the Axio Imager Z2 (Zeiss, Oberkochen, Germany), equipped with a 63× NA 1.4 oil-immersion objective and an AxioCam MRm charged-coupled device (CCD) camera (Zeiss). Confocal microscopy was performed using an LSM980 microscope equipped with AiryScan 2.0 (Zeiss). Image acquisition of primary neurons and brain sections was performed in AiryScan SR-4Y sampling mode using a Plan-Apochromat 63×/1.40 Oil DIC M27 objective. For calcium imaging, excitation was at 435 nm and emission at 660 nm, with the LD LCI Plan-Apochromat 25×/0.8 Imm Korr DIC M27 objective and sampling Mode CO-8Y at 200 ms per frame. For direct comparison, samples were imaged in parallel and using identical acquisition parameters.

QUANTIFICATION AND STATISTICAL ANALYSIS

Quantitative bioimaging

Image analysis was performed using Fiji, ICY,[86] IMARIS (version 9.5.0), and CellProfiler software version 4.2.1.

Quantification of object-based colocalization (<5 pixels), puncta density, intensity, and size was done with the ComDet v.0.5.5 plugin for Fiji. The ComDet segmentation parameters, based on intensity threshold and particle size, were kept constant whenever possible, and small adjustments were made to accommodate differences in labeling. When needed, images were preprocessed with the "subtract background" command in Fiji. ComDet was also used to measure the integrated intensity of Bin1 puncta in the colocalizing synaptic puncta in neurons or brain slices.

For the analysis of Bin1 puncta in somatic and distal regions, the ComDet plugin was used in the axonal ROI obtained with the "Segmented line" and "Straightener" IJ tools.

To determine the impact of KCl stimulation on the intensity of axonal Bin1, the ICY software was used to outline the axons and measure the mean intensity of Bin1 after background subtraction. Subsequently, the mean intensity of Bin1 was measured in ROIs defined by thresholding vGLUT1 or vGAT using Fiji.

For neurons expressing Bin1-Myc, synaptic density measurements were performed using ICY software. Within the "Spot detector" tool, a region of interest (ROI) was defined based on the Myc channel. Segmentation parameters were adapted for each image. The number of synaptic puncta and the area of the segmented ROI were extracted to calculate synaptic density. To measure colocalization between Bin1 wild-type or mutants and synaptic markers, the ComDET plugin was used on ROIs outlined using the polygon tool in Fiji.

The size of presynaptic Rab5 endosomes was extracted using a CellProfiler pipeline set up in the lab. Rab5, vGAT, and vGLUT1 puncta intensity were processed using enhanced operation (feature type speckles). Puncta were identified by applying the ''Identify Primary objects'' module. Subsequently, Rab5 puncta was selectively masked in vGAT or vGLUT1 puncta. The masked Rab5 area was exported using the ''Measure Object Size Shape'' function. A similar pipeline was used to measure the size of presynaptic Rab5 endosomes in Bin1-Myc-expressing neurons. Myc intensity was processed using ''enhance'' (feature type neurites) and segmented by ''Threshold''. Following synapsin I and Rab5 puncta identification with ''Identify Primary objects,'' synapsin I puncta were masked within the Myc signal. Then, Rab5 was masked within the synapsin I-masked signal. The area of the resulting masked Rab5 was quantified using the ''Measure Object Size Shape'' tool and exported.

Neuronal morphology in neurons overexpressing MYC-tagged plasmids was assessed using the Simple Neurite Tracer plugin (SNT) and Sholl analysis.[95] In neurons knockdown of Bin1, neuronal morphology was skeletonized and analyzed using the ''Analyze Skeleton'' Fiji plugin.[96]

Statistics

GraphPad Prism version 8.4.0 was used to represent individual replicates with mean ± SEM and statistical analysis. All experiments were carried out in at least three independent sets of cultures. The sample size was determined based on the results of pilot studies. Outliers were removed by the ''Identify Outliers'' function (ROUT method) in GraphPad. The data were tested using the D'Agostino-Pearson omnibus normality test. The Wilcoxon matched-pairs signed rank test was applied for non-parametric and paired data, or the Friedman test for multiple comparisons. The Ordinary one-way ANOVA or unpaired t test was used for parametric and unpaired data. For parametric and unpaired data, the Mann-Whitney test was applied; For non-parametric and unpaired data, the Kruskal-Wallis test was applied, as specified in figure legends.